Applied Energy 348 (2023) 121600

Contents lists available at ScienceDirect

Applied Energy

journal homepage: www.elsevier.com/locate/apenergy

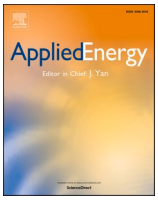

A fuel cell range extender integrating with heat pump for cabin heat and power generation

Nan Zhang, Yiji Lu [*,1], Sambhaji Kadam, Zhibin Yu [1]

James Watt School of Engineering, University of Glasgow, Glasgow G12 8QQ, UK

HIGHLIGHTS

- Develop a novel vehicle energy system to extend DR and ensure cabin comfort.
- Integrated waste heat recovery system connecting HP, battery and backup FC.
- Analyse the system using 4E methods from a macro vehicle perspective.
- Comparative study across EVASHP, PTC baseline and proposed novel system.

GRAPHICAL ABSTRACT

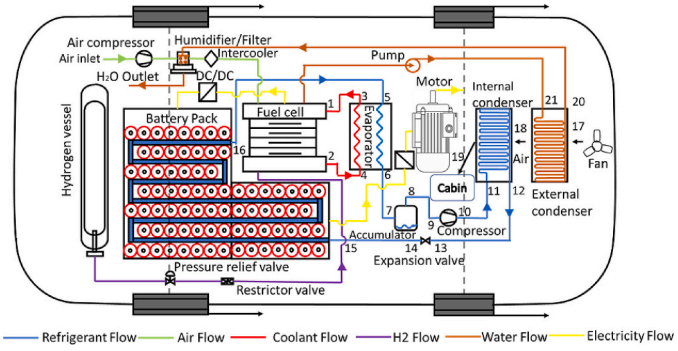

ARTICLE INFO

Keywords:
Integrated energy system
Heat pump
Fuel cell
Battery
Advanced thermal management

ABSTRACT

Batteries, Heat Pumps (HPs), and fuel cells (FCs) are critical for transport decarbonization and a net zero future. However, cabin heating in extreme conditions leads to severe driving range reduction in current Electric Vehicles (EVs). The performance of the heat pump (HP) in EVs and its performance enhancement technologies are widely investigated but cannot, simultaneously, provide sufficient heat and high COP. The source and amount of the waste heat within a vehicle for the heat pump integrated system is a crucial challenge to improve performance. The structure becomes increasingly complicated, but the benefits are not significant. Therefore, in this study, a small Fuel Cell, battery and heat pump integrated energy management system for range extended EVs (FCBEEV) is designed. The cogeneration characteristic of the fuel cell and waste heat from battery pack are utilised by the heat pump to ensure a high-level of cabin comfort in extremely cold temperatures and an extension of the driving range. A numerical model was established in MATLAB and the results were analysed from energy, exergy, environment, and economic (4E) perspectives. In this study, we show that the highest COP_{sys} of the proposed system is 5.8 and can improve the driving range (DR) by 65% to 110% compared to the reference systems. The exergy efficiency of the suggested system is 75% at −10 °C and the fuel cell and internal condenser are the primary causes of the exergy destruction. The environmental impact decreases by 13 kg/year per car compared to current EVs with a Positive Temperature Coefficient (PTC) and Air Source Heat Pump (ASHP) system, and the reduction is primarily sourced from the indirect emissions. The operating cost which includes driving and heating is 28.9% higher than cited for an ASHP and PTC system and 41% higher than the PTC baseline system.

* Corresponding author.
E-mail addresses: yiji.lu@glasgow.ac.uk (Y. Lu), zhibin.yu@glasgow.ac.uk (Z. Yu).
[1] The two authors have the same contribution to this study.

https://doi.org/10.1016/j.apenergy.2023.121600
Received 22 November 2022; Received in revised form 20 June 2023; Accepted 13 July 2023

The payback duration is 300,000 km at current market prices, and it is predicted to be shorter to 100,000 km, if the cost of the fuel cell stack is estimated at £4000 and the H_2 price is the same as electricity. We anticipate that the proposed system can significantly improve cabin comfort and driving range anxieties, as well as promote the decarbonization of transport.

Nomenclature

Symbols

A	area [cm^2] for fuel cell [m^2] for heat exchanger
a	acceleration [m/s^2]
Bo	boiling number
C_{O2}	oxygen concentration at the catalyst interface
C_O	convective number
Cp	specific heat capacity [J/ (kg K)]
Cv	EEV flow coefficient
Cd	drag coefficient
D_h	hydraulic diameter [m]
e	chemical exergy [kJ/kg]
E	exergy [J]
E_{nerst}	open-circuit reversible voltage [V]
F	Faraday's constant 96,485 [coulombs/mol] or force
Fr	Froude number
g	gravitational acceleration 9.8 [m/s^2]
Ga	Galileo number
h	heat transfer coefficient
H	enthalpy [J/kg]
i	current density [A/cm^2]
i_{fg}	enthalpy of vaporization [J/kg]
I	current[A]
Ja	Jakob number
k	conductivity
l	thickness [cm]
$\dot{m}$	Mass flow rate [kg/s]
M	molecular weight [kg/mol]
M_{veh}	vehicle weight [kg]
Nu	Nusselt number
P	partial pressure [atm]
Pr	Prandtl number
Q	heat [W]
$\dot{q}$	Specific energy [MJ/kg]
R	universal gas constant 8.31447 [kPa·m3/(kmol·K)]
Re	Reynolds number
R_{wall}	wall heat transfer resistance
S	entropy [J/(kg·K)]
T	temperature [K]
T_0	reference temperature [K]
U	total heat transfer coefficient
v	velocity [m/s]
V	voltage [V]
V_a	activation voltage [V]
V_c	concentration voltage [V]
W	energy consumption [W]
x	mole fraction
X	vapour quality
X_{tt}	turbulent-turbulent Lockhart Martinelli parameter

Greek symbol

ω	stoichiometry
λ	conductivity [W/(m·K)]
δ_{wall}	thickness of the plate [m]
ρ	density [kg/m^3]
μ	dynamic viscosity [Pa·s]
η_0	overall surface efficiency
η_{isen}	isentropic effectiveness
φ	void fraction
γ	compressing ratio
ε	efficiency
θ_{leak}	leakage rate

Subscripts

annular	annular flow
amb	ambient
bat	battery
cab	cabin
cg	charging
chr	battery charging
cl	coolant
comp	compressor
cond	condenser
cs	cross-section
dis	compressor discharging
dch	battery discharging
des	destruction
dr	drag resistance
driving	driving perspective
econd	external condenser
eva	evaporator
exv	expansion valve
fc	fuel cell
f_{rr}	rolling coefficient
FC	fuel cell stack
gr	gradient resistance
h	hot
hp	heat pump
heat	heating perspective
H_2	Hydrogen
H_2O	Water
i	inlet
icond	internal condenser
IHX	internal heat exchanger
lab	labour
lo	liquid only
m	mean
mod	module
nernst	nernst open circuit
ohm	ohmic losses
o	outlet
op	operating
O_2	oxygen
OC	open circuit
OHX	external heat exchanger
ref	refrigerant
rr	rolling resistance
ser	series
sys	system
tf	traction force
veh	vehicle

wall	wall of heat exchanger
wavy	wavy flow
wo	water only

Acronyms

AC	alternating current
ACC	additional capital cost
ASHP	air source heat pump
BEV	battery electrical vehicle
BC	initial battery pack capacity
CC	capital cost
COP	coefficient of performance
CPFC	cost per fully charging cycle
DC	direct current
DRE	driving range extension
DRER	driving range extension rate
EEBC	equivalent effective battery capacity
EEV	electronic expansion valve
EOC	effective operating cost
EV	electrical vehicle
EVASHP	electrical vehicle air source heat pump
FCBEEV	fuel cell battery range-extended electrical vehicle
GWP	global warming potential
LMTD	logarithmic mean temperature difference
PEMFC	proton-exchange membrane fuel cell
PP	payback duration
PWHR	percentage of waste heat recovery
PTC	positive temperature coefficient
SOC	state of charge
TEWI	total equivalent warming impact
WLTD	worldwide harmonized light vehicles test cycle

1. Introduction

Climate changes has become the greatest challenge for the human race. COP26 stressed the critical target of maintaining any temperature increase within 1.5 °C [1]. CO_2 is considered as the largest contributor to global warming, with 20% of direct CO_2 emissions from fuel combustion coming from road vehicles [2]. To comply with the net zero target, many countries and governments have committed to reach 100% Zero Emission Vehicle (ZEV) new sales between 2030 and 2050, including Norway which plans to ban the sale of fossil fuel vehicle by 2025, and Germany by 2030 [3]. Therefore, ZEVs, such as Battery Electric Vehicles (BEVs) and Fuel Cell Electric Vehicles (FCEVs) will see explosive growth in the foreseeable future. However, the reduction in driving range caused by heating systems in extreme cold weather has plagued consumers and hindered the development of decarbonization. It is estimated that the heating load for cabin at −20 °C is in the range of 3.3 kW to 6.8 kW [4]. However heating the cabin with a Positive Temperature Coefficient (PTC) heater will cause a reduction of 30% in driving range within one charging cycle, compared to summer condition [5]. Therefore, in recent years, developing high efficiency heating technologies for EVs has gained increasing attention worldwide.

The Air Source Heat Pump (ASHP), that is largely utilised in domestic heating, is considered as a suitable alternative to the PTC heater. It can utilise low grade heat in the low temperature ambient air for cabin thermal comfort [6]. Lee et al. [7] studied the performance of an R134a heat pump system for EVs at −10 °C which can provide 3.1 kW heat with a COP of 3.26. They also evaluated the exergy of their designed heat pump system, in which the internal condenser had the greatest exergy destruction. A similar system with a larger compressor and heat exchanger was applied to large passenger EVs which only had a COP of 2.4 at 10 °C [8]. Qin et al. [9] discussed the performance of an R134a EVASHP at −20 °C, and the results demonstrated that a minimum COP of 2.1 with a maximum heating capacity of 3.3 kW can be achieved. Due to the space limitations in EVs, conventional ASHP cannot provide sufficient heat with high COP under extreme cold weather conditions. Some researchers have investigated alternative refrigerants to improve the heating performance in extreme cold conditions and reduce the GWP of the refrigerant, whilst avoiding structural modifications. Direk et al. [10] used R1234yf instead of R134a, and the results indicated that the system can provide up to 2.6 kW heat with a COP of 4 at 5 °C. Yu et al. [11] investigated the performance of three new-developed refrigerants by comparing them to R410a, namely M1 (R32/R1123/R161/R13I1 (22%/35%/8%/35%)), M2 (R32/R1123/R161/R13I1 (22%/30%/13%/35%)) and M3 (R32/R161/R13I1 (22%/48%/30%)). The COP of M3 increased by up to 22% compared to R410a, but only 1.65 kW heating capacity can be achieved at −10 °C. A CO_2 and CO_2 mixture have also been frequently discussed in recent years. Dong et al. [12] conducted an experimental study into CO_2 heat pump for EVs. The results proved that CO_2 heat pump could successfully provide over 6 kW heat but only had a COP of 2.1 at −20 °C. Similar heating capacity can also be found in Ref. [13] but the COP is even lower. Additionally, Yu et al. [14] evaluated the performance of a CO_2/R41 mixture. They assumed that the higher the R41 mass fraction, the lower the heat capacity would be, but the COP would be marginally improved A number of researchers have attempted to introduce vapour injections technologies to EVASHP in order to improve the performance. Qin et al. [15] experimentally investigated a R134a heat pump using a compressor with two different injection portholes. It can be concluded that with the vapour injection, the heating capacity can be improved by 28.6% compared to the traditional system but the COP reduced by a maximum of 25%. Jung et al. [16] conducted research on the impacts of an injection port on performance and suggested that the COP could be improved by 7.5% and 9.8% respectively when a single injection port and dual injection port are set to be 440° and 535/335°. Yang et al. [17] introduced a vapour injection CO_2 heat pump system to EVs. The authors claimed that the proposed system can work within the range −30 °C to 50 °C, but the maximum heating capacity at −30 °C was only 2.2 kW and the COP was 1.45. However, the vapour-injection technology was still able to improve the performance by 75.7% at −30 °C, compared to basic system. However, a serious problem is regularly ignored when considering the performance of a heat pump, namely frost formation on the Outdoor Heat Exchanger (OHX). Steiner et al. [18] highlighted out that, at 0 °C, the COP declined dramatically after the first 15 min frosting period and reduced by 30% after 25 mins while the compressor power consumption increased by 50%. Zhou et al. [19] reversed the heat pump cycle and utilised the heat in the vehicle to defrost the OHX without considering the cabin comfort. Li et al. [20] designed a secondary loop to prevent the frost formation. However, the heat source of the secondary loop is from a PTC heater. Additionally, Liu et al. [21] also optimized the heat pump system from the heat exchanger perspective to achieve a better temperature uniformity in the OHX which can delay frosting at low temperatures. Similarly, Mahvi et al. [22] modified the surface wettability of an aluminium louvered-fin heat exchanger that commonly used in vehicles and the results show that it can successfully delay the frost formation at −0.7 °C with a 3 kW heating capacity and a COP of 2.1. Jung et al. [23] investigated the impact of the length of the Internal Heat Exchanger (IHX) and claimed that the optimal COP of 2.7 occurred when IHX's length was 300 mm.

Although significant efforts have been undertaken to develop EVASHP, it is likely that the heat pump cannot meet the high COP and high heating capacity simultaneously, and the frosting problem is difficult to address. Hence, many researchers believe integrated energy systems are vital for delivering various energy services [24]. Ahn et al. [25] developed a dual source heat pump by using air and waste heat in

EVs. They concluded that the heating capacity and the COP increased by 31.5% and 9.3% respectively compared to pure ASHP at 0 °C with 2.5 kW waste heat. It was also highlighted that the performance at −10 °C was highly dependent on the amount of waste heat. However, as the waste heat in the paper was simulated by an electric heater, it was unknown whether there was sufficient waste heat in EVs. Han et al. [26] investigated the heating performance of a ASHP for an electric bus. According to the results, the improvement could be achieved when the waste heat was over 2 kW, and the ambient temperature was below 0 °C. Tian et al. [27,28] did a series of research studies focused on the integrated thermal management system. They considered using the waste from the motor and collectively evaluated the energy, exergy, and economic performance. The highest COP achieved was 2.75 with 1 kW waste heat from the motor with a temperature at −7 °C and the system maximum exergy efficiency was 40%. Lee et al. [29] experimentally studied a muti-level waste heat recovery vapour injection heat pump system for EVs. Different from the conventional parallel waste heat recovery system, the refrigerant absorbed the waste heat and was injected into the vapour injection compressor at a middle pressure. The results demonstrated that the system proposed by Lee could improve the COP by 6.6% at −20 °C but the COP started lower than conventional systems when the ambient temperature was higher than −5 °C.

In summary, the EVASHP cabin heating system and its performance enhancement technologies, including different refrigerants, vapour injection, and frost formation prevention have been widely discussed. However, considering the heat pump separately from the whole vehicle system cannot provide sufficient heating capacity and high COP simultaneously. Some researchers investigated the heat pump integrated system by using waste from the battery pack or motor. Although the performance can be improved when ambient temperature is in the range of −10 °C to 0 °C and when the waste heat is over 1 kW, for most scenarios, the waste heat is provided by the PTC heater and the practical waste heat is at different temperatures under unknown operating conditions. Additionally, devices that perform well at very low temperatures often perform poorly at high temperatures or may not even function at high temperatures, due to compressor limitations. Compared with ordinary systems, units with full-scale compressors have lower COP and heating capacity over the entire operating range. The most important issue is the severe frosting problem which will mean the heat pump cannot provide stable heating capacity all the time and is sensitive to the ambient temperature. Furthermore, very few studies tried to analysis the integrated system from a whole vehicle perspective, research has been largely undertaken only from heat pump perspective. Therefore, further research on how to provide sufficient and stable heat with high COP, extending the driving range, and avoiding the effects of frost and compressor limitation is still necessary and crucial. Additionally, analysis from the whole vehicle perspective should be adopted to evaluate the performance from a macro perspective.

As summarised above, despite the growing interest in EVASHP development technologies and integrated systems, challenges remain to be addressed in terms of efficient cabin heating, CO_2 emissions and driving range reduction. In order to address these challenges, this study proposed a highly integrated energy system by integrating a fuel cell stack, a battery pack, and a heat pump. The cogeneration characteristic of the fuel cell was adopted so that not only the electricity generated by the fuel cell could be used but also the waste heat from the fuel cell stack can be utilised as a stable heat source for cabin heating. A refrigerant-based BTMS was adopted to simplify the system and reduce the exergy deduction. The coolant heat pump was adopted instead of the traditional air source heat pump to recover the waste heat from the fuel cell and battery to maintain their operating temperature and supply stable heating loads to the cabin. The proposed system could operate with high COP, extend the Driving Range (DR) of EVs and reduce CO_2 emissions. An acceptable payback period could be achieved due to the lower operating costs. Moreover, the proposed system can be further utilised in other areas such as domestic or city heating systems, and provide ideas for future heat and electricity cogeneration energy management systems.

2. System description

The schematic diagram of the proposed system is shown in Fig. 1. Different colours represent different flows, for example, the blue line represents for the refrigerant flow, the green line represents the fuel cell supply air flow, the red line represents the coolant flow, the purple line symbolizes the H_2 flow, brown line symbolizes water flow, and the yellow line represents electricity flow. The arrows on each line demonstrate for the flow direction. The proposed system has three key

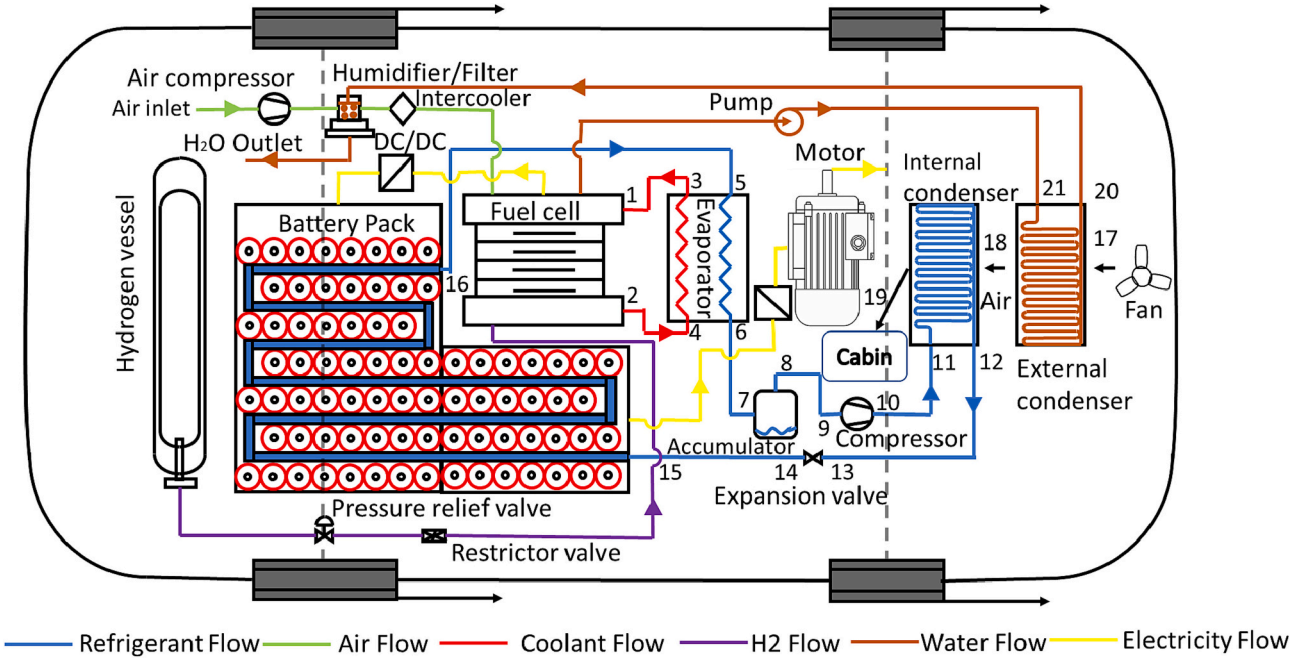

Fig. 1. Schematic diagram of the heat pump assisted energy management system for FCBEV.

subsystems: the fuel cell, the battery, and the heat pump. The fuel cell subsystem includes a fuel supply circuit, a coolant cooling cycle, and a DC/DC power output. In the fuel supply circuit, the supply air passes the air compressor to reach the working pressure but needs to pass through the humidifier and intercooler in order to be further cooled and humidified before entering the fuel cell stack. The pressure of the H_2 stored in the Hydrogen vessel is much greater than the working pressure in the fuel cell stack, hence it is necessary to reduce the pressure of the supplied H_2 before reacting in the fuel cell stack. The operating temperature of the fuel cell stack is controlled by a coolant loop which carries the heat from the fuel cell stack and releases it in the evaporator. The power generated from the reaction is supplied to battery pack via a DC/DC while the by-product of the reaction, water, flows through the external condenser to pre-heat the air supplied to the cabin and cools and humidifies the supplied air to the fuel cell, and finally discharges to the outside. The battery cycle contains a battery pack, a refrigerant based cooling system, a DC/AC, and a motor. From a thermal management perspective, the refrigerant flows into the cold plates inside the battery pack to maintain the operating temperatures of the batteries and finally enters the evaporator as a mixture. Meanwhile, as the main power supplier of the vehicle, the battery also needs to supply electricity via a DC/AC to the motor, but the difference is that it can, simultaneously, also receive power from the fuel cell. The heat pump cycle includes an evaporator, an internal condenser, a refrigerant compressor, and an expansion valve. The refrigerant enters the evaporator to absorb the heat released by the high temperature coolant from the fuel cell stack, to help the coolant complete a full cycle and becomes saturated refrigerant vapour. Whereafter, the vapour refrigerant passes by the compressor and enters the internal condenser to heat the preheated cabin supply air up to the setpoint and finally, the refrigerant passes through the expansion valve to complete a whole cycle. In the proposed integrated thermal management system, the heating capacity of the heat pump is designed to match the heat generated from the battery pack and fuel cell stack in order to always maintain their optimal operating temperature. As the battery pack is still the main power source of the vehicle, the current output of which is decided by different driving scenarios while the fuel cell only works as a power supplement. Therefore, the current output of the fuel cell stack will be actively adjusted to meet different cabin heating demands. With the proposed energy management system, the battery pack and fuel cell stack can always operate under optimal conditions, the heating demands can always be covered and at the same time, the driving range is extended with the power output from the fuel cell stack.

3. Model development

3.1. PEM fuel cell energy model

The Proton-Exchange Member (PEM) fuel cell is an electrochemical device that converts the chemical energy of fuels such as hydrogen and oxygen into electrical energy and heat. The voltage of a fuel cell can be calculated as:

$$V_{fc} = E_{nerst} - \Delta V_{ohm} - \Delta V_a - \Delta V_c \tag{1}$$

in which E_{nerst} is the open-circuit reversible voltage, ΔV_{ohm}, ΔV_a and ΔV_c are the ohmic voltage drop, the activation voltage drops, and the concentration voltage drop respectively. E_{nerst} can be expressed as below [30]:

$$E_{nernst} = 1.228 - \left[0.85 \times 10^{-3} \times \left(T_{fc} - 298.15\right) - 4.3086 \times 10^{-5} \times T_{fc} \times ln\left(P_{H_2} \times {P_{O_2}}^{0.5}\right)\right. \tag{2}$$

where T_{fc} is the temperature of a fuel cell, P_{H_2} and P_{O_2} are the pressures of hydrogen and the partial pressure oxygen in the air respectively. The ohmic voltage drop can be simply modelled by Eq. (3):

Table 1
Parameters for fuel cell model [35].

Specification	Value	Unit
Fuel cell operating temperature	65	°C
Inlet O_2 pressure P_{O_2}	2.5	atm
Inlet H_2 pressure P_{H_2}	0.504	atm
Current output I_{FC}	190–230	A
Number of cells N_{FC}	40	/
Area of cell A_{FC}	285.8	cm^2
Thickness of cell l_{FC}	5.1×10^{-3}	cm

$$\Delta V_{ohm} = R_{ohm} \times i_{fc} \tag{3}$$

where R_{ohm} is the specific fuel cell resistance (Ωm^2) which can be achieve in Ref. [31, 32] and i_{fc} is the current density of a fuel cell (A/m^2) which is formulated as below:

$$i_{fc} = \frac{I_{FC}}{A_{FC}} \tag{4}$$

in which, I_{FC} is the current output of the fuel cell stack and A_{FC} is the surface area of the fuel cell stack. The activation voltage drop ΔV_a is given as following:

$$\Delta V_a = -\left(\alpha_1 + \alpha_2 \times T_{fc} + \alpha_3 \times T_{fc} \times ln(C_{O_2}) + \alpha_4 \times T_{fc} \times ln(i_{fc})\right) \tag{5}$$

α_{1-4} are the coefficient of activation losses which can be obtained from Ref. [33] while the C_{O_2} is the concentration of oxygen which can be determined by Henry's law [34]. The equation of the concentration voltage drop ΔV_c is defined as below:

$$\Delta V_c = \frac{3 \times R \times T_{fc}}{4 \times F} \times ln\left(1 - \frac{i_{fc}}{i_{fc\_max}}\right) \tag{6}$$

where i_{fc_max} is the maximum current density of a fuel cell which is assumed equal to $2.2*10^{-4}$ (A/m^2) [35], and R is the universal gas constant, while F is the Faraday constant.

According to the voltage of a fuel cell and open circuit voltage, the heat generation and the power output of a fuel cell stack can be calculated as below:

$$Q_{FC} = N_{FC} \times I_{FC} \times \left(E_{nerst} - V_{fc}\right) \tag{7}$$

$$P_{FC} = N_{FC} \times V_{fc} \times I_{FC} \tag{8}$$

where N_{FC} is the number of the fuel cell in the fuel cell stack. Addi-

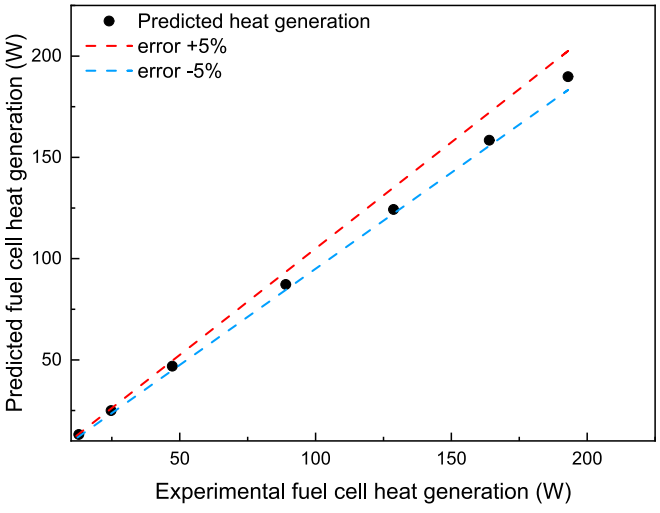

Fig. 2. Fuel cell heat generation model validation by comparison with experimental data in Ref. [35].

Table 2
Specifications for battery model [39].

Specification	Value	Unit
Battery capacity	8	Ah
Battery voltage	4.2	V
Number of batteries	2436	/
Number of batteries in series for one module	6	/
Number of batteries in parallel for one module	29	/
Number of modules	14	/
SOC	0.5	/
Battery operating temperature	30	°C
Voltage of battery pack	352	V
Battery pack capacity	60	kWh

tionally, the fuel mass flow of hydrogen and air and the produced H_2O are calculated as below [36,37]:

$$\dot{m}_{H2} = \frac{Q_{FC} + P_{FC}}{\dot{q}_{H2}} \times 10^{-3} \tag{9}$$

$$\dot{m}_{air} = 3.57 \times 10^{-7} \times \omega \times \frac{P_{FC}}{V_{fc}} \tag{10}$$

$$\dot{m}_{H_2O} = \dot{m}_{H_2} \times \frac{M_{H_2O}}{M_{H_2}} \tag{11}$$

where, $\dot{q}_{H2}$=120 MJ/kg is the specific energy of hydrogen and M_{H_2O} and M_{H_2} are the molecular weight of H_2 and H_2O.

Therefore, the power consumption of the air compressor in fuel cell supply system is given by:

$$P_{FC,comp} = \dot{m}_{air} \times Cp_{air} \times \frac{\Delta T}{\varepsilon_{FC,comp}} \tag{12}$$

where $\varepsilon_{FC,comp}$ is the mechanical efficiency of the air compressor, which is assumed to be 90% in this study. The parameters of the fuel cell selected in this study are shown in Table 1. and the fuel cell heat generation model validation is shown in Fig. 2.

3.2. Battery energy model

The simplified heat generation model of a battery cell while the battery is discharging is formulated as below:

$$Q_{bat} = \underbrace{I_{dis}^2 \times R_{dis}}_{irreverssible} - \underbrace{I_{dis} \times T_{bat} \times \frac{dE_{OC_{bat}}}{dT_{bat}}}_{reverssible} \tag{13}$$

where I_{dis} and R_{dis} is the current and the battery internal resistance respectively while discharging. $\frac{dE_{OC_{bat}}}{dT_{bat}}$ is the entropy coefficient, and the experimental data can be found in ref. [38]. The heat generated during charging by the fuel cell stack can be determined using the same equation as used for the discharging process. The power input from the fuel cell stack is defined as:

$$P_{chr} = I_{FC} \times \frac{V_{FC}}{N_{ser} \times V_{bat} \times N_{mod}} \tag{14}$$

While the discharging power is considered as:

$$P_{dis} = I_{dis} \times N_{par} \times N_{ser} \times V_{bat} \times N_{mod} \tag{15}$$

in which V_{bat} is the voltage of a battery, N_{ser}, N_{par} represent the number of cells in parallel and that in series for each string respectively while N_{mod} refers to the number of modules in the battery pack. The 60-kWh battery pack in this study is designed based on a 2013 Tesla model S and the specifications are shown in Table 2.

The predicted battery model was validated by comparing the heat generation and internal resistance while charging and discharging with Ref. [38] as shown in Fig. 3.

3.3. Heat exchanger model

In the proposed system, there are three heat exchangers. One of them is the plate heat exchanger which is used as an evaporator while the other two are fin and tube heat exchangers.

For the evaporator, the overall heat transfer coefficient U_{eva} can be calculated as:

$$\frac{1}{U_{eva}} = \frac{1}{h_{cl}} + \frac{1}{h_{eva,ref}} + \frac{\delta_w}{\lambda_w} \tag{16}$$

where, h_{cl}, $h_{eva,ref}$ is the heat transfer coefficient for coolant side and refrigerant side respectively while λ_w is the plate conductivity and δ_w is the thickness of the plate. The h_{cl} is adopted from Ref. [40]:

$$h_{cl} = 0.2121 \times Re_{cl}^{0.78} \times Pr^{1/3} \times \left(\frac{\mu_m}{\mu_{wall}}\right)^{0.14} \times \left(\frac{k_{cl}}{D_{h,eva}}\right) \tag{17}$$

in which Re_{cl} is the Reynolds number for coolant flow, Pr is the Prandtl number, μ_m and μ_{wall} are the dynamic viscosity calculated based on the coolant bulky temperature and wall temperature. In addition, $D_{h,eva}$ is the hydraulic diameter of the plate heat exchanger and k_{cl} is the conductivity of coolant. For the refrigerant side, the $h_{eva,ref}$ is depicted as [41]:

$$h_{eva\_ref} = 1.055 \times \left[1.056 \times Co^{-0.4} + 1.02 \times Bo^{0.9}\right] \times X_m \times h_{lo} \tag{18}$$

where Co is the convective number and Bo is the boiling number. X_m is the mean vapour quality in the evaporator and the h_{lo} is the heat transfer coefficient for pure liquid phase refrigerant which can be obtained in Ref. [41].

For the fin and tube internal and external condenser, the overall heat transfer coefficient is formulated as:

$$\frac{1}{U_{cond}A_{cond}} = \frac{1}{\eta_0 \times h_c \times A_c} + R_{wall} + \frac{1}{\eta_0 \times h_h \times A_h} \tag{19}$$

in which η_0 is the overall surface efficiency which can be achieved in Ref. [42]. In this study, for the internal condenser, the hot side is the refrigerant side while the cold side is the air side. Similarly, for the external condenser, the fluid on cold side is still air while the fluid on the hot side becomes water. The heat transfer coefficient for the refrigerant side is different depends on the speed of the flow. For the wavy flow, the Nusselt number (Nu_{wavy}) is defined as [43]:

$$Nu_{wavy} = \frac{0.23 \times Re_{vo,ref}^{0.12}}{1 + 1.11 \times X_{tt}^{0.58}} \times \left[\frac{Ga \times Pr_l}{Ja_l}\right]^{0.25} + cos^{-1}(2 \times \varphi - 1)/\pi \times 0.0195 \times Re_l^{0.8} \times Pr_l^{0.4} \times \sqrt{1.376 + c_1/X_{tt}^{c_2}} \tag{20}$$

in which c1 and c2 is determined by the Froude number (Fr), X_{tt} is the turbulent-turbulent Lockhart Martinelli parameter, Ga is the Galileo number, Ja_l is liquid Jakob number, and φ is the void fraction which is illustrated in Ref. [44]. For the annular flow, the expression of $Nu_{annular}$ is:

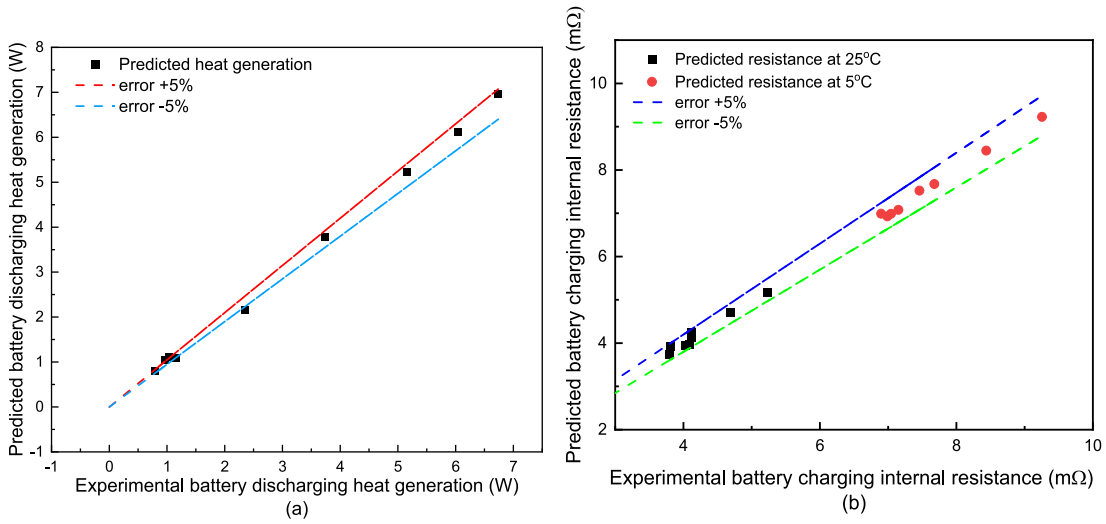

Fig. 3. Battery energy model validation by comparison with the experimental data in Ref. [38].

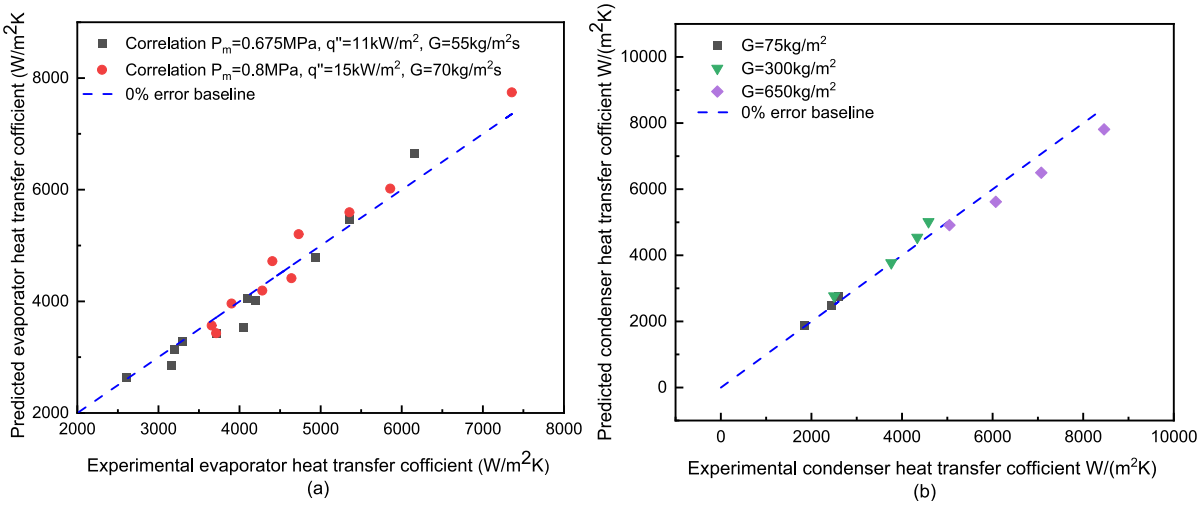

Fig. 4. Heat exchanger model validation (a) evaporator by comparison with experimental data in Ref. [40] and (b) condenser by comparison with experimental data in Ref. [43].

$$Nu_{annular} = 0.023 \times Re_l^{0.8} \times Pr_l^{0.4} \times \left[1 + \frac{2.22}{X_{tt}^{0.89}}\right] \tag{21}$$

For the external condenser, as there is only one phase water in the tube, Nu_{wo} is defined as:

$$Nu_{wo} = 0.023 \times Re_{wo}^{0.8} \times Pr_{wo}^{0.4} \tag{22}$$

For the air side, a simple heat transfer model is adopted as introduced in Ref. [42]:

$$h_{air\_cond} = C \times Re_{air}^{m} \times Pr^{1/3} \tag{23}$$

where C and m is determined by the air speed. The heat balance across the evaporator and condensers is formulated as below:

$$Q_{eva/icond/OHX} = \dot{m}_{cl/air/H_2O} \times Cp_{cl/air/H_2O} \times \Delta T_{cl/air/H_2O} \tag{24}$$

$$Q_{ref} = \dot{m}_{ref} \times (1 - X_{inlet}) \times i_{fg} \tag{25}$$

$$Q_{eva/cond/econd} = U_{eva/icond/econd} \times A_{eva/icond/econd} \times LMTD_{eva/icond/econd} \tag{26}$$

where the logarithmic mean temperature difference (LMTD) and i_{fg} is the enthalpy of vaporization of the selected refrigerant R134a. The validations for both heat exchanger models are shown in Fig. 4 with errors within 5%.

3.4. Compressor and expansion valve model

The compressing ratio (γ) and the compressor power consumption are important. Kinab et al. [45] concluded the relationship between refrigerant temperature and mass flow rate for a fixed compressor speed:

$$\begin{aligned} m_{ref} =& b_0 + b_1 t_{eva} + b_2 t_{eva}^2 + b_3 t_{eva}^3 + b_4 t_{cond} + b_5 t_{cond}^2 + b_6 t_{cond}^3 + b_7 t_{eva} t_{cond} \\ &+ b_8 t_{eva}^2 t_{cond} + b_9 t_{eva} t_{cond}^2 \end{aligned} \tag{27}$$

in which coefficients b_0 to b_9 can be obtained from Ref. [27]. In this study, the refrigerant evaporating and condensing temperature are related to the pressure via REFPROP and the equation is solved by using MATLAB code. The validation of compressor model is conducted by comparing with the results in Ref. [46], as shown in Fig. 5 and the average error is within 5%. The power consumption of the compressor is shown as below:

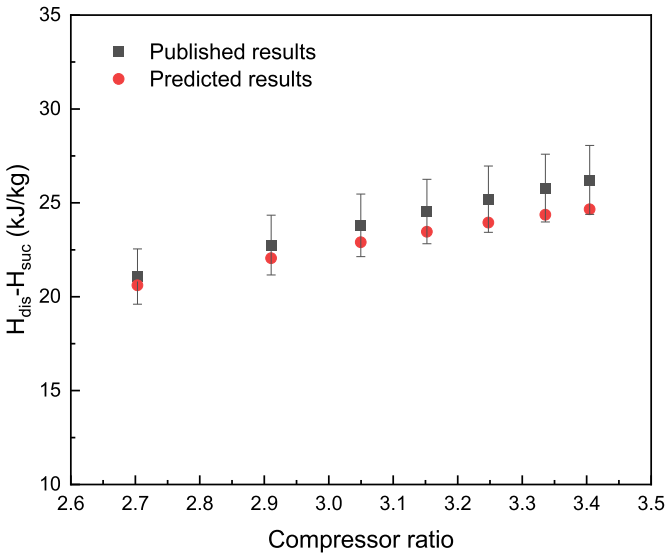

Fig. 5. Compressor model validation by comparison with experimental data in Ref. [46].

$$W_{comp} = \frac{\dot{m}_{ref} \times (H_{dis} - H_{suc})}{\eta_{isen}} \tag{28}$$

in which H_{dis} and H_{suc} are the enthalpy of R134a at the suction and exit of the compressor respectively, η_{isen} is the isentropic effectiveness of the compressor which is assumed to be 0.67 [47].

The process by which the refrigerant passes by the expansion valve is considered an adiabatic process. During the process, the enthalpy is unchangeable. The mass flow rate through the EEV is calculated as Ref. [28]:

$$\dot{m}_{EEV} = C_v A_c \sqrt{2 \times \Delta P_{EEV} \times \rho_{ref\_in}} \tag{29}$$

whereA_c is the circulation area while C_v is the flow coefficient, and $C_v = 0.02005 \times \sqrt{\rho_{in}} + 0.634/\rho_{out}$.

3.5. Vehicle motion model

According to Newton's second law, the vehicle longitudinal motion is defined as below:

$$F_{net} = M_{veh} \times a_{veh} \tag{30}$$

in which, F_{net} is the net Force on the vehicle, M_{veh} is the mass of the vehicle while a_{veh} refers to the vehicle's acceleration. Additionally, based on the principle of force balance, F_{net} can also be expressed as:

$$F_{net} = F_{tf} - F_{dr} - F_{rr} \pm F_{gr} \tag{31}$$

where F_{tf}, F_{dr}, F_{rr}, F_{gr} are the traction force (N), aerodynamic drag resistance (N), rolling resistance (N), and gradient resistance (N). Among them, F_{gr} can be ignored when the vehicle is only driven on a flat road. The expression of the aerodynamic drag resistance is given as following:

$$F_{dr} = 0.5 \times A_{cs} \times \rho_{air} \times C_d \times (v_{veh} \pm v_{wind})^2 \tag{32}$$

in which, A_{cs} is the cross-section area of the vehicle (m^2), C_d stands for the drag coefficient for the targeted Tesla model 3 [48]. v_{veh} and v_{wind} refer to the speed of vehicle and wind (m/s) and their relationship depends on their directions. F_{rr} is defined as:

$$F_{rr} = f_{rr} \times M_{veh} \times g \times cos\theta \tag{33}$$

where f_{rr} is the coefficient of rolling resistance, which is decided according to the tyres used on a Tesla Model 3. [49] and the results from Ref. [50] and $cos\theta$ is 1 in our scenario. The traction power from the battery is formulated as follows:

$$P_{bat} = \frac{(F_{tf}{}^* v_{veh})}{\varepsilon_p} \tag{34}$$

where ε_p is the powertrain efficiency which is assumed to be 0.95 [51]. The total battery power output is considered as:

$$P_{bat,total} = P_{bat} + P_{aux} \tag{35}$$

in which P_{aux} refers to the auxiliary power, including the power for the heat pump system, the power for the air pre-processing system, and the pump power consumption. The adopted Tesla Model S specifications and other components are listed in Table 3.

The model is validated based on the test EPA Coast-Down testing results concluded by Haye and Goodarzai [37]. The numerical results of the traction power under different vehicle speeds, shown in Fig. 6, show an error within 3% compared to the test results.

Table 3
Vehicle and components specifications.

Parameters	Symbol	Value
Vehicle		
Cross-section area [49]	A_{cs}	1.69*1.43 m^2
Drag coefficient [48]	C_d	0.23
Powertrain efficiency [51]	ε_p	0.95
Rolling coefficient [50]	f_{rr}	0.0084
Weight [49]	M_{veh}	2100 kg
Fuel cell [32,52]		
Fuel cell Operating temperature T_{FC}		65 °C
Inlet O_2 pressure	P_{O_2}	2.5 atm
Inlet H_2 pressure	P_{H_2}	2.4 atm
Number of cells	N_{FC}	40
Area of cell	A_{FC}	285.8 cm^2
Thickness of cell	l_{FC}	5.1 × 10^{-3} cm
Other devices		
Fuel cell evaporator		
	Number of plates	110
	Plate size	120 × 330 mm^2
	Channel space	2.9 mm
Internal condenser		
	inner diameter	7 mm
	Internal area	2.086 m^2
	External area	8.344 m^2
Air preheat condenser		
	Inner diameter	8.2 mm
	Internal area	0.2865 m^2
	External area	0.3725 m^2
Inverter Compressor		
	Displacement	27 cc/rev
	Compressor speed	3000–5000 rpm

3.6. Energy performance indicators

Coefficient of Performance (COP) is an important indicator to evaluate the efficiency of an energy system. According to the definition of COP and the characteristic of proposed integrated system, a COP for System (COPS) is defined as below:

$$COP_{sys} = \frac{Q_{cab,heat} + Q_{bat,cool} + Q_{FC,cool}}{W_{ref,comp} + W_{air,comp} + W_{pump} + W_{fan}} \tag{36}$$

where $Q_{cab,heat}$, $Q_{bat,cool}$ and $Q_{FC,cool}$ are the cabin heating capacity, battery cooling capacity, and fuel cell cooling capacity respectively while $W_{ref,comp}$, $W_{air,comp}$, W_{pump} and W_{fan} represent the power consumption of the heat pump compressor and power consumption of the air compressor for the fuel cell air supply, pump power consumption, and

fan power consumption respectively. The power consumption of fan and pump, W_{fan} and W_{pump} are calculated based on Ref. [53] and it is assumed that they are linearly related to the air and coolant velocity.

The Percentage of Waste Heat Recovery (PWHR) is defined as Eq. (37) which is used to evaluate the impacts of the waste heat in the vehicle thermal management system:

$$PWHR = \frac{Q_{FC} + Q_{battery}}{Q_{FC} + Q_{battery} + Q_{cab_{heat}}} \tag{37}$$

Driving Range Extension Rate (DRER) is a comparative indicator that can intuitively reflect the ratio of Driving Range Extension (DRE) of the selected system compared to Driving Range (DR) of conventional systems. It can be expressed as:

$$DRER = \frac{DRE}{DR} \tag{38}$$

3.7. Exergy analysis and indicators

Exergy analysis is also important as it helps evaluate an energy management system meaningfully and rationally. It indicates the maximum useful work that can be achieved from the whole system when the system changes reversibly from an arbitrary state to a state in equilibrium with a given environment. The general expression exergy flow is shown below:

$$\dot{E} = \dot{m} \times [(H - H_0) - T_0(S - S_0)] \tag{39}$$

in which H_0 and S_0 are the enthalpy and entropy respectively according to the reference temperature T_0 which is 0 °C in this study.

The exergy destruction for each component is the difference between the fuel exergy and production exergy of each component. For the heat exchanger, the fuel exergy is calculated by the state point of the refrigerant side while the production exergy is calculated by the state point of the fluid side [54]. The exergy destruction of heat exchangers including FC plate type evaporator, internal fin-tube type condenser, external condenser, and refrigerant battery pack cold plate are calculated by Eqs. (40) to (44) respectively:

$$E_{des\_eva} = m_{ref} \times [(H_5 - H_6) - T_0(S_5 - S_6)] + m_{cl} \times [(H_3 - H_4) - T_0(S_3 - S_4)] \tag{40}$$

$$E_{des\_inc} = m_{ref} \times [(H_{11} - H_{12}) - T_0(S_{11} - S_{12})] + m_{air} \times [(H_{18} - H_{19}) - T_0(S_{18} - S_{19})] \tag{41}$$

$$E_{des\_exc} = m_{ref} \times [(H_{20} - H_{21}) - T_0(S_{20} - S_{21})] + m_{air} \times [(H_{17} - H_{18}) - T_0(S_{17} - S_{18})] \tag{42}$$

$$E_{des\_beva} = Q_{bat} \times \frac{T_0 - \overline{T_{beva}}}{\overline{T_{beva}}} - m_{ref} \times [(H_{16} - H_{15}) - T_0(S_{16} - S_{15})] \tag{43}$$

where $\overline{T_{beva}}$ is the average temperature between the battery and the refrigerant.

The compressor's exergy destruction, caused by mechanical and electrical losses, is defined as Eq. (44):

$$E_{des\_comp} = W_{comp} - \{m_{ref} \times [(H_{10} - H_9) - T_0(S_{10} - S_9)]\} \tag{44}$$

where W_{comp} is the compressor power consumption, which is expressed in:

$$W_{comp} = \frac{(H_{10} - H_9)}{\eta_{isen}} \tag{45}$$

in which η_{isen} is the isentropic effiectiveness of the compressor which is assumed to be 0.67 [47]. The exergy destruction of expension valve (EXV) is desrcibed as Eq. (46) due to the constant enthalpy process:

$$E_{des\_exv} = m_{ref} \times T_0 \times (S_{14} - S_{13}) \tag{46}$$

For the fuel cell stack, except the general exergy flow metioned in Eq. (47), there is also chemical exergy occuring which can be calculated in terms of the following equation:

$$e^{CH} = \sum x_n \times e_n^{CH} + R \times T_0 \times \sum x_n \times ln x_n \tag{47}$$

where x_n is the mole fraction of the gas fuel. For H_2 the e^{CH} is considered as 119,044 (kJ/kg) [55] and the total exergy can be expressed as:

$$\dot{E}_{H2} = m_{H2} \times \left\{ C_{p,H2} \times T_0 \times \left[\frac{T}{T_0} - 1 - ln\frac{T}{T_0} + ln\left(\frac{P}{P_0}\right)^{\frac{k-1}{k}} \right] + e_{H2}^{CH} \right\} \tag{48}$$

For air, it consists of 77.48% N_2, 20.59% O_2, 0.03% CO_2 and 1.9% H_2O (g) and the total exergy is shown in Eq. (49) [56]:

$$\dot{E}_{air,FC} = m_{air,FC} \times \left\{ C_{p,air,FC} \times T_0 \times \left[\frac{T}{T_0} - 1 - ln\frac{T}{T_0} + ln\left(\frac{P}{P_0}\right)^{\frac{k-1}{k}} \right] + e_{air,FC}^{CH} \right\} \tag{49}$$

and the exergy of the water produced during the reaction can be calculated as:

$$\dot{E}_{H2O,FC} = m_{H2O} \times \left\{ C_{p,H2O,FC} \times T_0 \times \left[\frac{T}{T_0} - 1 - ln\frac{T}{T_0} + ln\left(\frac{P}{P_0}\right)^{\frac{k-1}{k}} \right] + e_{H2O}^{CH} \right\} \tag{50}$$

in which the e_{H2O}^{CH} is assumed as 51.212 kJ/kg [55]. Hence,the fuel cell exergy destruction can be fomulated as:

$$E_{des,FC} = \dot{E}_{H2} + \dot{E}_{air,i,FC} - \dot{E}_{H2O,FC} - \dot{E}_{air,o,FC} - P_{FC} - Q_{FC} \tag{51}$$

Hence, the total exergy destruction of the system is the sum of the irreversible loss of each component, which can be described as:

$$E_{des,sys} = E_{des,eva} + E_{des,inc} + E_{des,exc} + E_{des,beva} + E_{des,comp} + E_{des,exv} + E_{des,FC} \tag{52}$$

In this study, the exergy analysis is carried out with respect to component level and system level, namely, component relative irreversibility rate and system exergy efficiency. The component relative irreversibility is defined as the ratio of exergy destruction of each component to the total exergy destruction of the system, while the exergy efficiency is described as the ratio of the system exergy output to the system exergy. The expressions are shown below:

$$\eta_{ir,name} = \frac{E_{des,name}}{E_{des,sys}} \tag{53}$$

in which, the subscripts name represents the name of the component and $\eta_{ir,name}$ is the relative irreversibility of the selected component:

$$\eta_{sys} = \frac{P_{FC} + \overbrace{E_{exc,air,out} - E_{exc,air,in}}^{\text{net exergy output of external condenser}} + \overbrace{E_{inc,air,out} - E_{inc,air,in}}^{\text{net exergy output of internal condensor}}}{\underbrace{\dot{E}_{H2} + \dot{E}_{air,i,FC} - \dot{E}_{H2O,FC} - \dot{E}_{air,o,FC}}_{\text{System fuel exergy consumption}} + \underbrace{W_{ref,comp} + W_{air,comp} + W_{pump} + W_{fan}}_{\text{System power consumption}}} \tag{54}$$

where, P_{FC} is the power generated by FC, E_{H_2} and E_{O_2} stand for the exergy input of H_2 and O_2 respectively.

3.8. Environmental impacts indicators

The environmental impacts of H_2 and refrigerant usage in the backup fuel cell of the proposed system can be evaluated by adopting the concept of the Total Equivalent Warming Impact (TEWI). The $TEWI_{hp}$ is a parameter that can quantitatively evaluate the direct and indirect greenhouse gas emissions of the heat pump during the whole life cycle. The TEWI in this study is developed based on Ref. [57], including the Global Warming Potential (GWP) of the refrigerant (1430 for R134a),

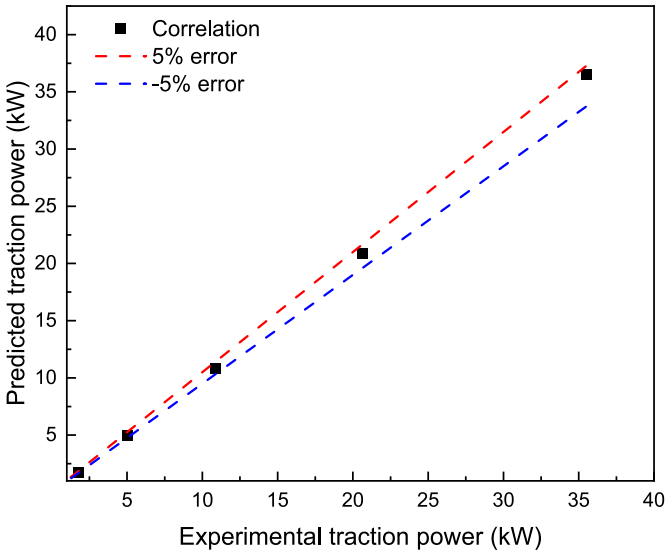

Fig. 6. Vehicle motion model validation by comparing with experimental data in Ref. [37].

the mass flow rate of the refrigerant for waste heat recovery and cabin heating, the annual emission of CO_2 due to the electricity consumption, and refrigerant leakage for chain heating. The expression of the $TEWI_{hp}$ is shown as follows:

$$TEWI_{hp} = GWP \times m_{ref_{chr}} \times \theta_{leak} \times t_{op,year} \times + GWP \times m_{ref_{chr}} \times (1-\alpha) + E_{hp} \times \beta_{elec} \times t_{op,year} \quad (55)$$

Furthermore, the vehicle level Total Equivalent Warming Impact per km ($TEWI_{DR}$) within one charging cycle is defined as

$$TEWI_{DR} = \left[GWP \times m_{ref_{chr}} \times \theta_{leak} \times t_{op,chr} \times N_{ch,year} + GWP \times m_{ref_{ch}} \times (1-\alpha) + P_{FC} \times \beta_{H_2} \times t_{op,ch} \times N_{ch,year} + E_{bat} \times \beta_{elec} \times N_{ch,year}\right] / DR_{total} \quad (56)$$

where $m_{ref_{chr}}$ is the refrigerant charging amount which is assumed to be 1.5 times the required refrigerant mass flow rate. θ_{leak} is the leakage rate of refrigerant from the heat pump and waste heat recovery system which is assumed as 4% according to the leakage rate range mentioned in Ref. [58]. $t_{op,chr}$ is the maximum operating hours of the selected scenario (6 kW heating capacity) per full charging cycle while $t_{op,year}$ is assumed as 100 h per year which is 1/4 of the annual driving hours in Ref. [59]. $N_{ch,year}$ stands for the charging times per year. α is the refrigerant recovery rate (%) which is considered as 0.85 according to Ref [60]. P_{FC} is the power generation of the fuel cell stack while E_{bat} is the power consumption of the battery. β_{H_2} is the CO_2 emission factor for H_2 used by the fuel cell which is shown in Table 4 while β_{elec} is the average CO_2 for producing electricity which is equal to 0.193 kg/kWh based on a report from the UK government [61].

3.9. Economic analysis and indicators

The economic analysis of the system is divided into three sections which are Capital Cost (CC), Additional Capital Costs (ACC), Effective Operating Cost (EOC), and Payback Period (PP).

Table 4
CO_2 emission factor for H_2 production under different methods [62].

Method of production	type	CO_2 emission factor (gCO_2/gH_2)	CO_2 emission factor for H_2 fuel cell (gCO_2/kWh)
Earth gas	Grey	7.05	375
Electrolysis of water	Mixed (black, brown)	34.68	1716
S-I cycle	Pink	10.34	1025

Table 5
Components comparison and capital costs.

Components	System in this study	Basic BEV system	Extra quantities	ACC
Cabin heating system				
Scroll compressor	●	●	0	
Water Pump	●	●	1	£53 [63]
Plate heat exchanger	●	●	Area difference	
Fin and tube heat exchanger	●	●	Area difference	
Refrigerant	●	●	Mass flow rate difference	
Pipe	●	●	0	
EXV	●	●	0	
Fan	●	●	0	
PTC	○	●	−1	£295 [64]
Liquid tank	●	●	0	
Fuel cell system [65]				
Fuel cell	●	○	1	£1234
Hydrogen tank (Type IV 350 bar)	●	○	1	£2399 [66]
Hydrogen supply system	●	○	1	£1196
Air supply system	●	○	1	£1034
Controls and instrumentation	●	○	1	£906
Electrical	●	○	1	£1956
Assembly components	●	○	1	£593
Battery system				
Battery pack	●	●	−33.7%	-£2710 [67]

The Additional Capital Costs (ACC) of the proposed FC backup thermal management system is defined according to the additional necessary components compared to basic EV with heat pump. The additional components and their Capital Costs (CC) are listed in Table 5.

The extra labour cost (ACC_{labour}) for assembly is considered 20% of the total ACC and the cost saving in the battery pack is due to the size scaled-down caused by the adopted small fuel cell stack. Hence, the ACC can be defined as:

$$ACC_{total} = \sum ACC_{name} \quad (57)$$

There are two aspects when evaluating EOC, and these are EOC for driving ($EOC_{driving}$) and EOC for heating (EOC_{heat}). The EOC is evaluated based on the ratio of the cost of Equivalent Effective Battery Capacity (EEBC) to the Cost Per Fully Charging (CPFC). The EEBC is defined as the available electricity in the battery pack that can be used for driving after considering the thermal management usage and FC charging. The expression of EEBC is shown below:

$$EEBC = BC - W_{hp} - W_{air,comp} - W_{pump} - W_{fan} + FC_{chr} \quad (58)$$

where BC, W_{hp} and FC_{chr} are the initial battery pack capacity, power comsuption of heat pump system, namely compressor power consumption, and supplemental battery capacity by fuel cell charging for a certain operating time respectively.

The CPFC is calculated by the amount and the price of H_2 and electricity price needed within one fully charging cycle. The O_2 needed by FC comes from air and is considered as free of charge:

$$CPFC = M_{H_2} \times CC_{H_2} + E_{bat} \times CC_{elec} \quad (59)$$

where M_{H_2} is the required H_2 quantity (kg) per charging cycle for a specific operating time and E_{bat} is the total battery energy consumption (kWh). CC_{H_2} is the price of H_2 which is assumed as 3.26 (£/kg) [68],

Table 6
Operating conditions in the simulation.

Parameter	Value	Unit
Ambient temperature (T_{amb})	−25 to 5	°C
Coolant inlet temperature at the entrance of evaporator ($T_{cl,eva,inlet}$)	27 to 33	°C
Fuel cell current output (I_{FC})	190 to 230	A
Battery discharging rate (C_{dch})	0.19 to 0.26	C

CC_{elec} is the average price of electricity which is 0.34(£/kWh) [69]:

$$EOC_{heat} = \frac{Q_{hp}}{CPFC_{heat}} \tag{60}$$

$$EOC_{driving} = \frac{EEBC}{CPFC_{driving}} \tag{61}$$

The PP calculated based on the driving range is determined by the ratio between operating cost saving and ACC_{total}.

$$PP = \frac{ACC_{total} \times t_{op} \times v_{veh}}{(EEBC_{FCBEV} - EEBC_{BEV}) \times CC_{elec} - (CPFC_{FCBEV} - CPFC_{BEV})} \tag{62}$$

3.10. Simulation procedure

The numerical simulation was conducted and coded in the MATLAB. The physical characteristics of the refrigerant R134a were obtained from REFPROP with MATLAB codes. The model included four main loops, namely, fuel cell, battery, evaporator, and condenser loop. Five independent inputs were set which were fuel cell current output, battery discharging C rate, evaporator coolant inlet temperature, ambient temperature, and subcooling degree and the associated operating range is shown in Table 6. The evaporator coolant inlet temperature variation range is set based on the operating range in Ref. [70]. The other parameters were considered as dependent variables which will be adjusted automatically with the changes in the five independent variables mentioned above, including but not limited to coolant, refrigerant and air mass flow rate, compressing ratio, outlet air temperature etc. Fuel cell temperature has the highest priority in the model. The model started with the fuel cell cooling system and evaporator in order to absorb all the heat generation from the fuel cell stack. Eqs. (24) to (26) is used to calculate the conservation of energy for each loop. Only when the error is lower than 0.0001, is the system considered convergent. The assumptions made in the simulation are shown below:

(1) Fuel cell stack coolant outlet temperature was fixed i.e. 30 °C.
(2) The pressure drop and heat loss across heat exchangers are neglected.
(3) The difference between the minimum temperature of the coolant in the evaporator and the R134a evaporating temperature is assumed as constant.
(4) Fuel cell stack's heat loss was ignored, but the heat loss of the battery pack was calculated under a constant air speed of 0.5 m/s according to the investigated battery discharging rate.
(5) The refrigerant entered the compressor is in saturated vapour and an accumulator was installed before the compressor to make sure only gas can enter the compressor.

4. Results and discussion

In this section, the performance of the proposed system under different fuel cell current output, cell discharge C rate, ambient temperature, and evaporator coolant inlet temperature is evaluated from four perspectives: energy, exergy, environment, and economy. The energy performance is assessed by COP_{sys}, COP_{hp}, PWHR, DR, and DRER while exergy is evaluated by exergy destruction, relative irreversibility,

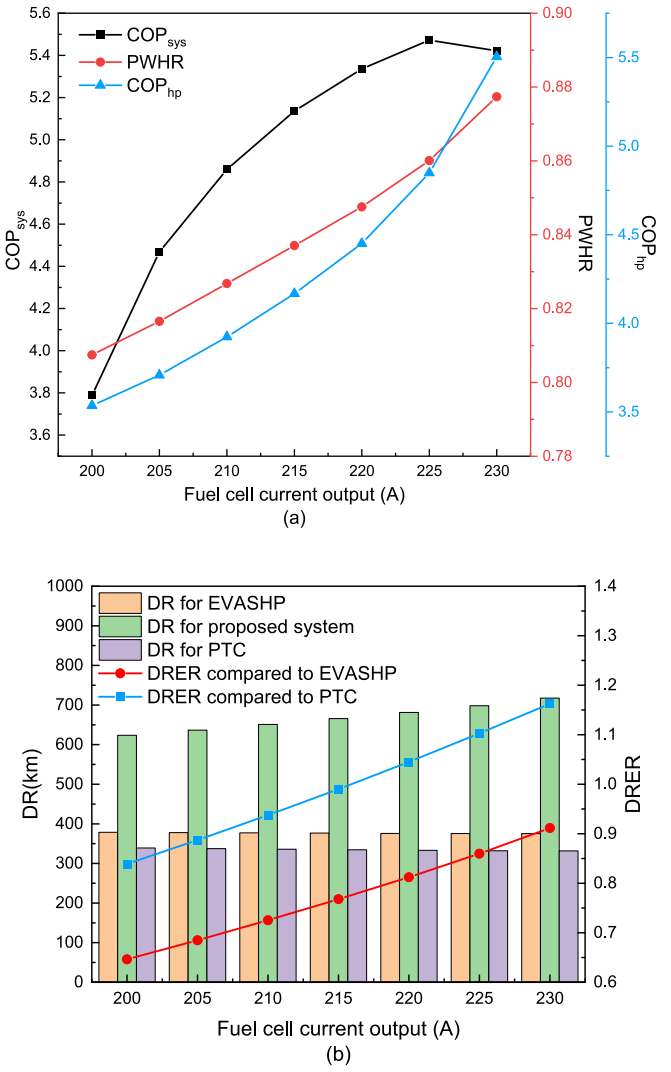

Fig. 7. The impacts of fuel cell current output on (a) COPsys, COP and PWHR (b) DR and DRER compared with EVASHP [13] and PTC ($T_{amb} = -20$ °C, $T_{cl,eva,inlet} = 30$ °C, $C_{dch} = 0.26$).

and exergy efficiency from the component level. Environment performance is estimated from $TEWI_{hp}$ and $TEWI_{DR}$ aspects and for the economic performance, ACC, EOC and PP are introduced. Furthermore, for more referable results and discussion, the results in this study are compared to some reported data regarding EVASHP and PTC baselines in published literature.

4.1. Energy analysis

Fig. 7 shows the impacts of fuel cell current outputs on the proposed system's energy performance regarding COP_{sys}, COP_{hp}, PWHR, DR, and DRER. In Fig. 7(a), with the increase of the fuel cell current output from 200A to 230A, the PWHR varies in the range of 0.807 to 0.877. This is because of the increasing heat generation in the fuel cell stack when the fuel cell current output increases, according to Eq. (7). The COP_{hp} is the traditional indicator for a pure heat pump system that has always been adopted in previous heat pump research. In the proposed system, the COP_{hp} rises from 3.53 to 5.5 as the fuel cell current output increases, however, although COP_{sys} also increases, the gradient of the increase gradually decreases and the COP_{sys} starts decreasing when the fuel cell current output exceeds 225A. The main reason for the difference is that in the COP_{hp} only W_{comp} is considered and the heat output from the internal condenser is the only useful power. However, in the COP_{sys}, the

power consumption of the fuel supply for the fuel cell, and the air supply for the cabin should also be considered. Moreover, from a system perspective, the heat supplied to the cabin and also the heat extracted from the fuel cell are both useful, as shown in Eq. (36). As a result, the COP_{sys} first increases with the increase of the fuel cell current output. However, due to the higher heating capacity and fuel cell current output, the power of the fan and fuel supply system is increased as there is an increase in air mass flow rate, H_2, and air feeding rate, resulting in a decrease in the gradient of the increase and even a decrease in COP_{sys}. In Fig. 7(b), it can be seen that the DR of the proposed system within one charging cycle increases from 623 km to 717 km when fuel cell current output varies from 200A to 230A. The increase in DR is primarily because of the rise in power supply from the fuel cell stack to the battery and the COP_{sys} shown in Fig. 7(a). Although the COP_{sys} decreases when the fuel cell current output exceeds 225A, the DR still increases as the increasing current can provide a higher supplement, compared to the increase in system power consumption. A comparison between the proposed FCBEEV system and the EVASHP system in Ref. [13] and the PTC baseline is conducted in Fig. 7(b). To provide the same heating capacity as the proposed system in this study, the DR of EVASHP shows a slight decrease caused by the increase in heating capacity. The DRER of the proposed system compared to EVASHP varies in the range of 0.646 to 0.911. The improvement compared to the PTC baseline is even higher and is between 0.83 and 1.16.

As shown in Fig. 8(a), when the battery discharging C rate increases, the COP_{sys}, PWHR and COP all increase correspondingly. The reason for the change in PWHR under different battery C rates is similar to that under different fuel cell current outputs. The increasing battery discharging C rate causes higher heat generation in the battery pack which will increase the waste heat ratio in total heating capacity. The COP_{hp} increases by 48% when the battery discharging rate varies from 0.2C to 0.29C. Apart from the extra heat provided by the battery pack, another reason is the increasing cooling demand of the battery leads to the decrease in refrigerant mass flow rate and inlet vapour quality of the refrigerant which reduces the compressor work relatively. The variation in COP_{sys} is different from that when changing fuel cell current outputs as there is no break point on the curve of COP_{sys} in Fig. 8(a). The explanation of the difference is that the increasing discharging C rate will not affect power consumption of fuel cell feeding system and hence has little impact on the total power consumption. Furthermore, although the battery discharging C rate leads to a rise in waste heat, the total heating capacity slightly decreases due to the compressor limits so that the fan power consumption does not experience as greater change as when changing fuel cell current outputs. Contrary to the trend of COP and PWHR, DR negatively correlated with battery discharging C rate. The DR of the FCBEEV in this study decreases dramatically compared to the DR of the previous EV with the ASHP system in Ref. [13]. To be specific, the DR of the previous EV with the ASHP system drops by only 12% while a 37% decline occurs in the proposed system. The reason is because as the battery discharging C rate increases, there is a corresponding reduction in the operating hours. Furthermore, the running resistance will increase in square according to Eq. (32) with the increasing of battery discharging C rate. However, different from traditional EVs, part of the DR of the proposed system comes from the

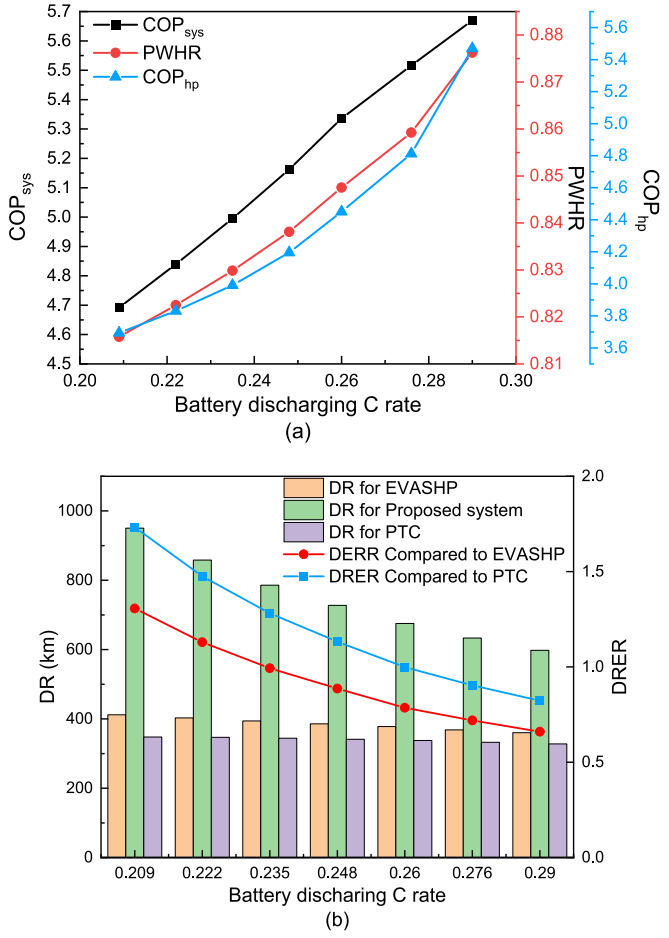

Fig. 8. The impacts of battery discharging C rate on (a) COPsys, COP, and PWHR (b) DR and DRER compared with EVASHP [13] and PTC ($T_{amb} = -20$ °C, $T_{cl,eva,inlet} = 30$ °C, $I_{FC} = 220$A).

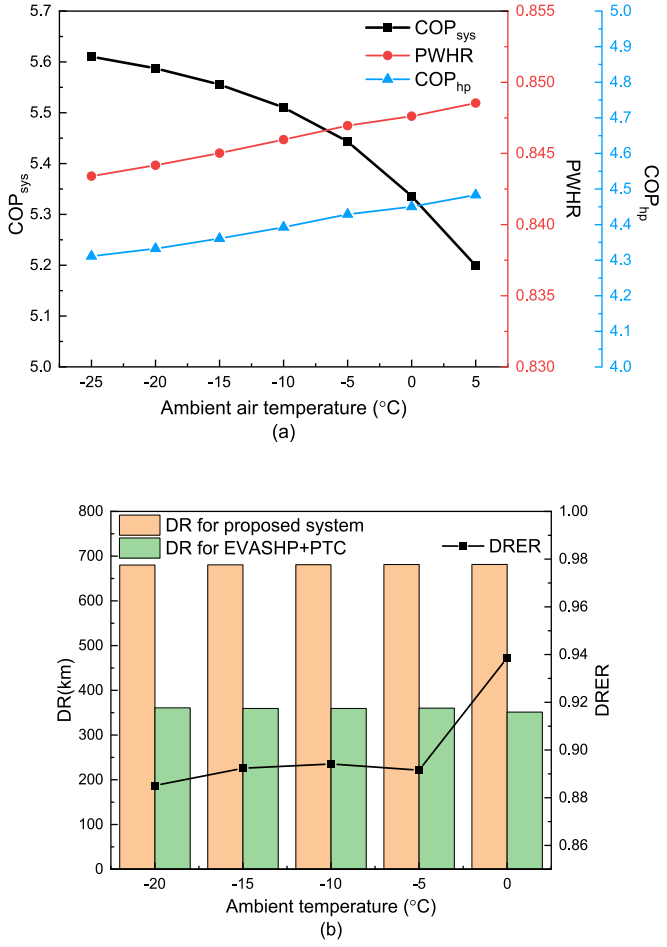

Fig. 9. The impact of battery discharging C rate on (a) COPsys, COP, and PWHR (b) DR and DRER compared with EVASHP [9] and PTC ($C_{dch} = 0.26$, $T_{cl,eva,inlet} = 30$ °C, $I_{FC} = 220$A).

fuel cell power supply and reduced operating hours with a fixed fuel cell power output leads to a decrease in DR. In addition, the advantage of the heat pump system also relies on the operating time which means the longer the operating time, the greater the benefits will be. Therefore, the DRER of the proposed system, compared to the EVASHP system and PTC baseline, declines with an increase of battery discharging C rate.

Fig. 9(a) illustrates the relationship between ambient temperature and the performance of the proposed system. It can be concluded that the proposed system is not sensitive to ambient temperature when considering PWHR and COP_{hp} as indicators. For instance, when the ambient temperature increases from −25 °C to 5 °C, the PWHR of the system and COP_{hp} only change by 0.5% and 3.9% respectively. This is because a coolant source heat pump is adopted instead of a conventional air source heat pump and consequently the performance of the heat pump largely depends on the temperature of the coolant rather than the ambient air temperature. Additionally, the heat loss of the fuel cell stack to the ambient is ignored. However, because of the lower temperature difference between the cabin inlet air and condensing temperature while increasing the ambient temperature, the air mass flow rate increases dramatically in order to absorb the same amount of heat from the internal condenser. Hence, the COP_{sys} reduced by 7% when the ambient temperature varies from −25 °C to 5 °C. In Fig. 9(b), an R134a vapour injection heat pump [9] is selected and compared to the proposed system in this study. Due to the insufficient heating capacity, a PTC heater should be applied to the reference heat pump system as a supplement. It can be seen that the DR of the proposed system is approximately 680 km

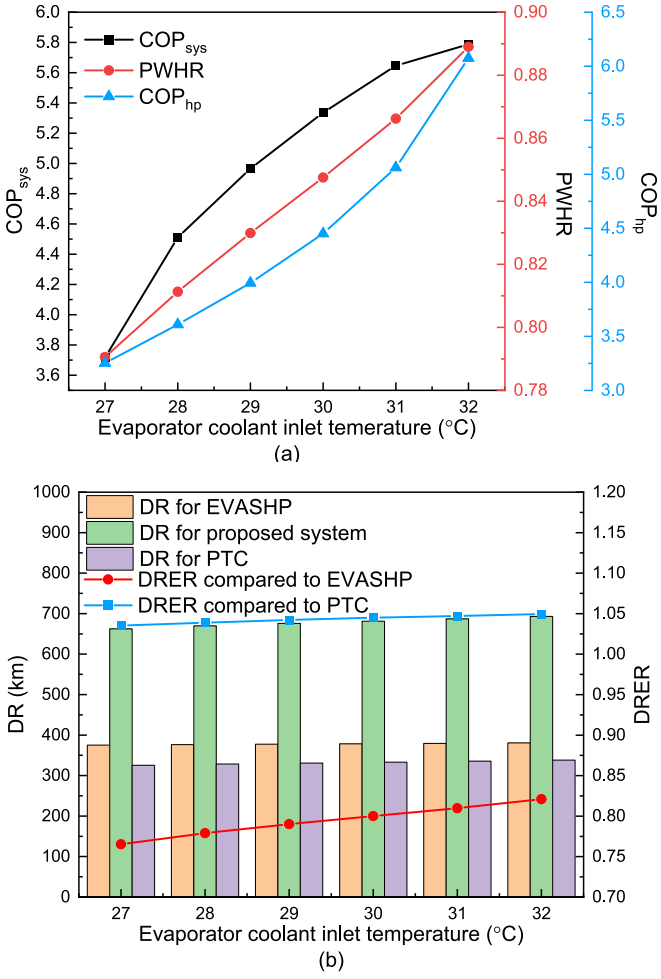

Fig. 10. The impacts of evaporator coolant inlet temperature on (a) COPsys, COP and PWHR (b) DR and DRER compared with EVASHP [13] and PTC (C_{dch} = 0.26, T_{amb} = −20 °C, I_{FC} = 220A).

irrespective of how the ambient temperature changes, and the DRER compared to the reference system is always over 0.88. It should be noted that the DR within one charging cycle of the reference system does not vary as significantly as the high battery discharge C rate and the impact of the temperature on DR will be much greater when the operating time within one charging cycle is longer.

Fig. 10 describes the influence of the evaporator coolant inlet temperature on the system performance. In Fig. 10(a), COP_{sys}, COP_{hp}, and PWHR are all positively related to the evaporator coolant inlet temperature. When the evaporator coolant inlet temperature increases from 27 °C to 32 °C, the PWHR rises from 0.79 to 0.89 correspondingly. The underlying reason is that, as the evaporator coolant inlet temperature increases, the coolant mass flow decreases and therefore the vapour mass of the post-EXV refrigerant decreases to maintain its cooling capacity. This series of changes will also reduce the refrigerant flow of the system and affect the compression ratio, thereby reducing the overall heating capacity under the condition that the waste heat remains unchanged. Similarly, with a decrease in refrigerant mass flow rate and compressor power consumption, the COP_{hp} increases by 86.8%, and the increasing rate of the change of COP_{hp} increases along with an increase in evaporator coolant inlet temperature due to the evaporator limitation. In contrast, the increasing rate of the change of the COP_{sys} shows a contrary trend compared to COP_{hp}. This is because although the power consumption of the coolant pump and compressor decreases, the cabin supply air speed should be increased to compensate for the deduction of the heat transfer coefficient of the refrigerant side of the internal condenser, according to Eqs. (19) and (26). In Fig. 10(b), it can be seen that due to the variations in COP, the DR of proposed system increases by 4.5% within one charging cycle while there is no impact on the DR of EV with ASHP system and PTC baseline as they do not have backup fuel cell systems. As a result, the DRER compared to those two traditional systems varies in the ranges of 1.03 to 1.05 and 0.765 to 0.82 respectively.

The results in Fig. 7 to Fig. 10 demonstrate that the proposed system can always provide a greater DR than the previous EVs with ASHP system and EVs with PTC baseline. In addition, fuel cell current output, battery discharging C rate, and evaporator coolant inlet temperature all have significant impacts on COP_{sys} and COP_{hp}. However, the influence caused by the ambient temperature is lower compared to the other three operating parameters. The difference indicates that proposed system is not sensitive to the ambient temperature so it can provide sufficient and stable heat to the cabin even in extreme cold weather. Furthermore, it can also be concluded that optimization of the fuel cell current output, battery discharging C rate, and evaporator coolant inlet temperature can help the system achieve a better performance. Moreover, only the battery discharging C rate and fuel cell current output have substantial effects on PWHR as they are directly related to the waste heat generation. Additionally, those two parameters also have an impact on DR. The higher the fuel cell current output, the higher the DR and DRER within one charging cycle, which can effectively improve the driving range concern while the battery discharging C rate shows a contrary trend. Therefore, a suitable relationship between fuel cell current output and battery discharging C rate should be built in order to achieve optimal DR.

4.2. Exergy analysis

Fig. 11 describes the exergy of the proposed system by considering it from component level and system level. As shown in Fig. 11(a), the system's total exergy destruction varies within the range 2791 W to 3079 W when the fuel cell current output rises from 200A to 230A. For the main components in the system, the exergy destruction of the compressor, internal condenser, EXV, and battery evaporator decrease while the exergy destruction of the evaporator, external condenser, and fuel cell increase. The reason for the increase in the evaporator is that the increasing fuel cell current output results in an increase of the

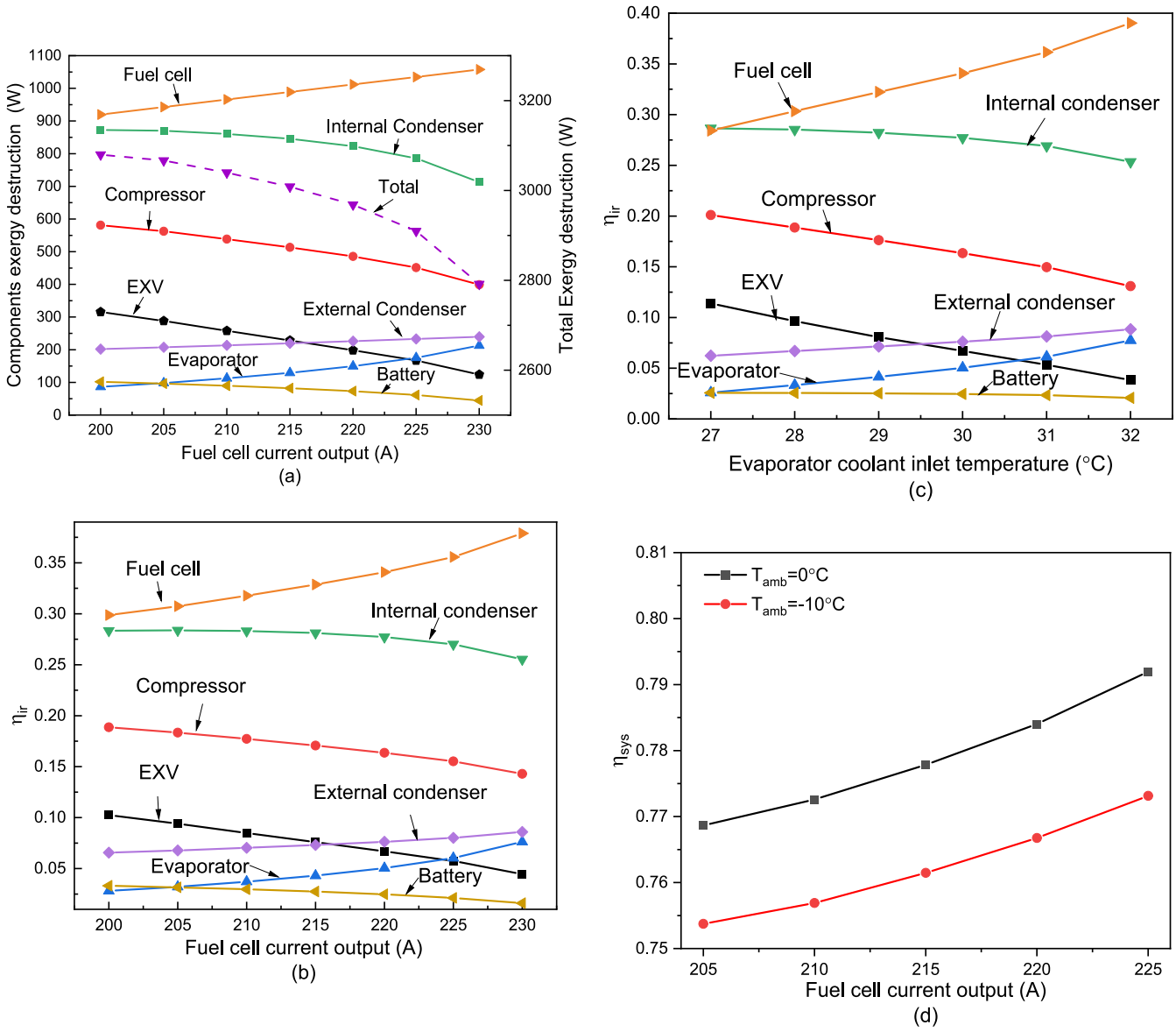

Fig. 11. The exergy of the proposed system.
(a) Exergy destruction (b) Relative irreversibility under different fuel cell current outputs. (c) Relative irreversibility under different evaporator coolant inlet temperatures (d) Exergy efficiency.

$LMTD_{eva}$ due to the increasing coolant mass flow rate. Similarly, the increasing fuel cell current output directly affects the fuel supply and the output of the fuel cell stack. An increased fuel consumption will result in an increased power output, and as a result the fuel cell exergy destruction increases. With regards to the decrease in the internal condenser exergy destruction, the decreasing condensing temperature profits from a reduction in temperature difference between cabin supply air side and refrigerant side. Furthermore, lower compressor power consumption, due to the growing refrigerant mass flow rate, causes a reduction in the exergy destruction of the compressor. Consequently, with the combined effect of all the above results, the exergy destruction of the system falls. Among all the components, the internal condenser and compressor play a decisive role. It is important to highlight that the fuel cell exergy destruction is much lower than a single fuel cell system. As well as the utilization of electrical power in the proposed system, waste heat from the fuel cell stack is also adopted.

Fig. 11(b) and (c) illustrates the variation of the relative irreversibility of each component under different fuel cell current outputs and evaporator coolant inlet temperatures. As depicted in Fig. 11(b), when the fuel cell current output increase from 200A to 230A, the irreversibility of the fuel cell suffers the greatest impact, it increases by 8.02% and always has the largest proportion of the total irreversibility. In addition, the relative irreversibility of the internal condenser, compressor, and EXV decrease by 2.8%, 4.57%, 5.8% respectively while the relative irreversibility of the external condenser and evaporator only increase by 2.03% and 4.82%. It can be seen that the relative irreversibility of the EXV is also very sensitive to the fuel cell current output as it has significant impacts on the condensing pressure and the refrigerant outlet vapour quality of the EXV. Furthermore, in Fig. 11(c), the impacts of the evaporator coolant inlet temperature on the components' relative irreversibility can be observed. The relative irreversibility of the fuel cell increases dramatically by 10.6%, when the evaporator coolant inlet temperature increases from 27 °C to 32 °C. The principle behind the impacts of evaporator coolant inlet temperature is different from that behind the impacts of fuel cell current output. When the evaporator inlet temperature changes, it does not affect the exergy destruction of fuel cell as there is no variation in its parameters. However, the total exergy destruction decreases which leads to an increase in the relative

irreversibility of the fuel cell. The EXV and compressor are the second and third most sensitive components with regards to the relative irreversibility, and a deduction by 7.56% and 7.01% can be achieved respectively. The main reason for this is the substantial decrease in relative irreversibility of the EXV and the compressor which is caused by the lower discharging temperature and pressure. In Fig. 11 (d), the exergy efficiency is presented from a system perspective in terms of the fuel cell current output and the ambient temperature. When the ambient temperature is constant and the fuel cell current output varies from 205A to 225A, the η_{sys} increase by 2.3% due to the lower exergy destruction in the sensitive components. Furthermore, the ambient temperature also has a particular impact on η_{sys} when the fuel cell current output is constant. When the ambient temperature deceases, the η_{sys} also decreases due to the larger temperature difference between the refrigerant side and air side. For example, at 220A fuel cell current output, the η_{sys} reduces by 2.2% when the ambient temperature decreases from 0 °C to −10 °C.

From Fig. 11, it can be concluded that fuel cell current output and evaporator make significant impacts on the exergy destruction and relative irreversibility by affecting internal parameters such as refrigerant mass flow rate, compressor pressure ratio, and temperature difference between the hot side and the cold side. Additionally, fuel cell current output and ambient temperature both have particular effects on η_{sys}. Potential improvements can be applied to the fuel cell stack, compressor, and internal condenser to reduce their exergy destruction in order to improve the η_{sys} or the operating parameters can be adjusted to achieve a greater η_{sys}.

4.3. Environmental analysis

Fig. 12 (a)-(c) describe the environmental impacts of the proposed system by introducing two indicators, namely $TEWI_{hp}$ and $TEWI_{DR}$. These two indicators assess the system from two different perspectives. The $TEWI_{hp}$ evaluates the environmental impacts from a heat pump perspective in terms of the operating hours while the $TEWI_{DR}$ analyses the environmental impacts from a macro perspective which consider the whole vehicle system in terms of the driving range. A comparison with current EV with PTC and ASHP [9] is made to demonstrate the advantages and disadvantages of the proposed system. As shown in Fig. 12(a), the total $TEWI_{hp}$ of the suggested system in this study is 370.5 kg while that for an EV with PTC and ASHP system is 383.8 kg. Among them, the direct emissions, which represent CO_2 emissions from the leakage and recovery of charged refrigerant, accounts for 88.7% of the total $TEWI_{hp}$, however, only 46% of the $TEWI_{hp}$ of the current EVs with PTC and ASHP system belongs to the direct emissions. This is due to waste heat recovery, all of which is transferred through the refrigerant, resulting in an increase in refrigerant mass flow and refrigerant charge, consequently leading to an increase in direct CO_2 emissions. In contrast, the indirect emission of the proposed system is much lower than the reference counterpart as the COP of proposed system is much higher. However, the difference of total annual $TEWI_{hp}$ among those two systems is not substantial, only 13 kg per year. Similarly, the gap in $TEWI_{DR}$ between the suggested system and reference system is also not significant. The proposed system can only achieve an improvement of 4.5% under the specific simulation conditions. Meanwhile, direct emissions of the proposed system are also higher than the reference counterpart while indirect emissions are lower. In order to further investigate the potential of proposed system on environment improvements, the impacts of GWP of the utilised refrigerant and the CO_2 emission factor for H_2 PEMFC on TEWI are discussed in Fig. 12(b) and (c). As displayed in Fig. 12(b), when alternative refrigerants with a lower GWP compared to R134a, which has a GWP of 1430, are adopted, the improvements on $TWEI_{hp}$ and $TEWI_{DR}$ will be greater. For instance, when the GWP of the refrigerant decreases from 1000 to 1, the $TEWI_{hp}$ of proposed system varies from 271.79 kg to 42.1 kg. Although the $TEWI_{hp}$ of EVs with a heat pump and PTC system can also be improved, descending from 330.33 kg

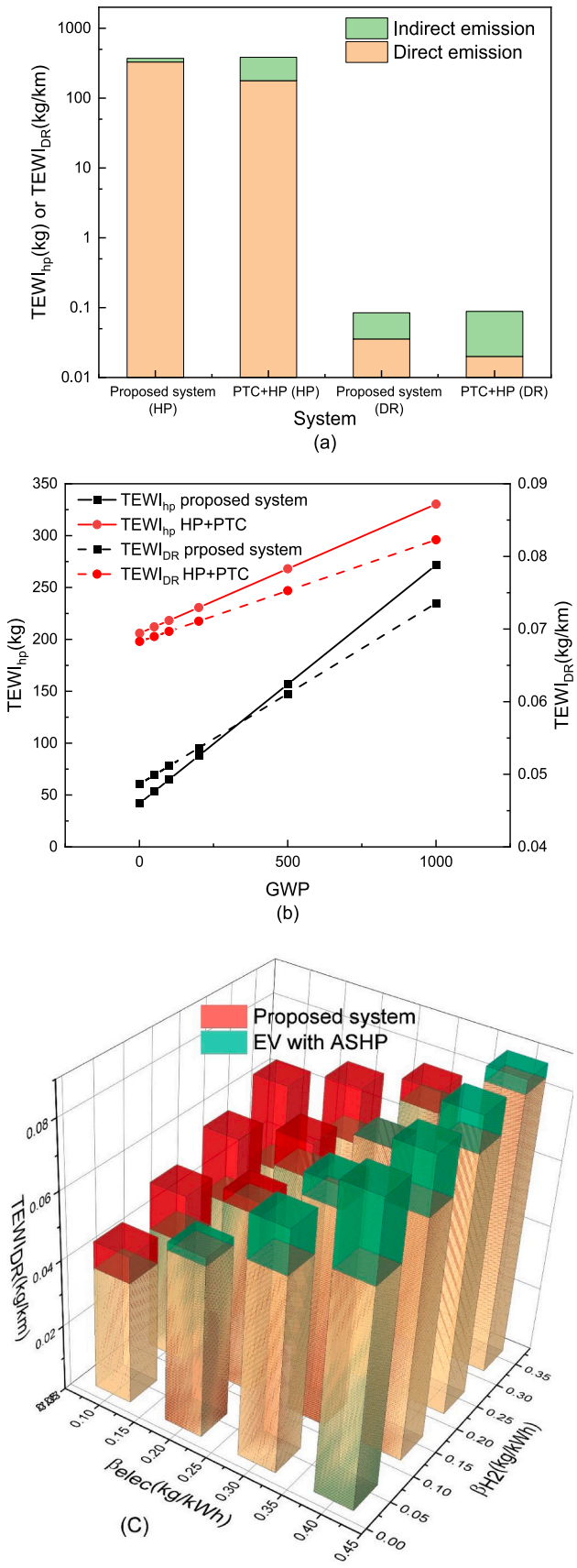

Fig. 12. Environmental (TWEI and $TEWI_{DR}$) analysis and comparison. (a) different systems (b) different refrigerants (GWPs) (c) different CO_2 factor.

to 205.96 kg, the gap between the proposed system and EVs with a heat pump and PTC system will be greater. The improvement rate varies in the range of 17.8% to 79.5%. This is because the vast majority of carbon emissions from the proposed coolant heat pump system are from direct emissions rather than indirect emissions, such as traditional EVASHP, as shown in Fig. 12(a). Similar impacts can be found on the $TEWI_{DR}$. The $TEWI_{DR}$ reduces by 34% when the GWP of the refrigerant changes from 1000 to 1. However, $TEWI_{DR}$ of the proposed system does not drop as fast as $TEWI_{hp}$ in conjunction with the decrease in GWP. The reason for this is because, with the exception of the refrigerant, some of the CO_2 emissions of the proposed system also come from the source of the H_2. It should be mentioned that the leakage rate is the main factor that causes the direct emissions, so if it can be well controlled, the proposed system could offer a better performance under the same conditions. Fig. 12(c) depicts how the CO_2 factor of electricity and H_2 affect $TWEI_{DR}$. It can be seen that the CO_2 factor of electricity and H_2 both have substantial impacts on $TEWI_{DR}$. For example, when β_{elec} is 0.3 kg/kWh, β_{H2} is 0.24 kg/kWh, the $TEWI_{DR}$ of the proposed system and EVs with ASHP and PTC system is 0.07115 kg/km and 0.07124 kg/km respectively. However, when β_{elec} and β_{H2} is 0.1 kg/kWh and 0.04 kg/kWh respectively, the $TEWI_{DR}$ of the proposed system will be 0.04494 kg/km while that of EVs with ASHP and PTC system will be 0.0371 kg/km. Therefore, for the refrigerant R134a, only when the β_{H2} and the β_{elec} meet a specific ratio range which should at least lower than 85% in this study, the proposed system can achieve advantages in $TEWI_{DR}$ compared to reference PTC and ASHP system. It should be noted that when using lower GWP refrigerants as alternatives, the acceptable ratio range will be wider.

According to the environmental analysis, the proposed system displays a significant advantage in indirect emissions but a disadvantage in direct emissions. The GWP of the refrigerant is more important to the proposed system than the reference EVASHP and PTC system. Hence, identifying lower GWP alternatives is important to achieve both lower $TEWI_{hp}$ and $TEWI_{DR}$. Another potential method to reduce the $TEWI_{DR}$ is to reduce the CO_2 factor during the production of H_2. It should be noted that the CO_2 factor during the production of H_2 and electricity need to meet certain ratio requirements for the benefits to be gained. For some Nordic countries, the requirements of the CO_2 factor during the production of H_2 are more stringent.

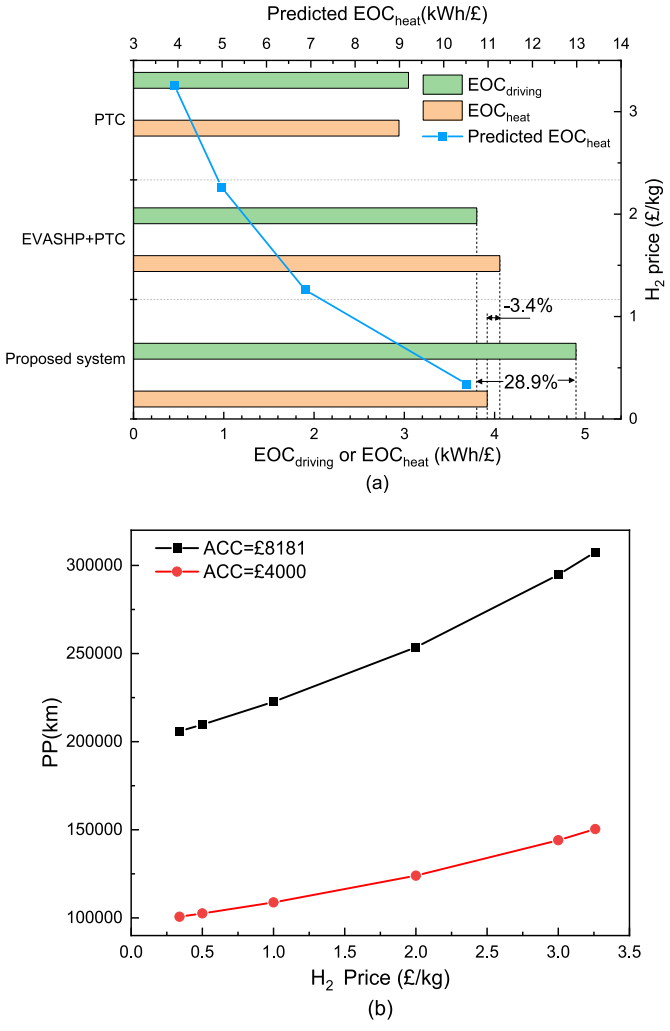

Fig. 13. Analysis of system economic performance. (a) $EOC_{driving}$ and EOC_{heat}, (b) PP (C_{dch} = 0.26, $T_{cl\_eva\_inlet}$ = 30 °C, I_{FC} = 220A, T_{amb} = 0 °C).

4.4. Economic analysis

In this section, an economic analysis is carried out by investigating the $EOC_{driving}$, EOC_{heat}, and PP. In Fig. 13 (a), a comparison of $EOC_{driving}$ and EOC_{heat} within one charging cycle under specific conditions for the proposed system, EVASHP and PTC combined system [9] and PTC system is described. For the proposed system, the $EOC_{driving}$ is 4.9kWh/£ while the figure is 3.8 kWh/£ and 3.2 kWh/£ for EVASHP and PTC combined system and pure PTC system respectively and the $EOC_{driving}$ of the proposed system is 28.9% higher than the reference EVASHP and PTC system. For the EOC_{heat}, the proposed system is 3.4% lower than the reference system but still much higher than the PTC baseline. This is because when the CPFC for the proposed system is calculated, the consumption of H_2 is also included. Although the COP of the proposed system is higher than the reference system, the reduction in electricity consumption cannot cover the increase in H_2 consumption. However, the H_2 consumption does not only provide enough heat, but also supplies power to the battery pack to extend the driving range which leads to a higher $EOC_{driving}$ in the proposed system. Additionally, further investigation on the EOC_{heat} is conducted to understand how the H_2 price affects it. The result shows that when the H_2 price decreases from £3.26 to £0.34 the highest EOC_{heat} is 1.69 times the lowest EOC_{heat}. According to the ACC, the PP is shown in Fig. 13(b). When the ACC is £8181 which is the most up to date price, the PP (measured in the driving distance) is 300,000 km based on the most up to date H_2 price. However, when the H_2 price is equal to the current electricity price, the PP reduces to 205,000 km. If the ACC of £4000 can be achieved through a decrease in price of the fuel cell system, the PP at the H_2 price of £3.26 and £0.34 will be 150,000 km and 100,000 km respectively. Considering the typical lifespan of a vehicle which is 250,000–300,000 km or 25 years [71], the proposed system just reaches the upper limit. For commercial vehicles, the annual driving distances can reach 80,000 km to 10,000 km per year [72]. Therefore, a reduction in the cost of the fuel cell system or the H_2 price, would allow the PP to be more competitive and attractive, particularly for commercial vehicles.

5. Conclusions

In this study, a highly integrated heat pump assisted battery electric vehicle with fuel cell backup energy management system was proposed and evaluated to improve the heating performance in extreme cold climates and eliminate anxiety associated withdriving range. A numerical model was developed, and the results were compared to the existing published systems. A detail assessment from energy (COP_{sys}, COP_{hp}, PWHR, DR, DRER), exergy (E_{des}, η_{ir}, η_{sys}), environment ($TEWI_{hp}$, $TEWI_{DR}$) and economic ($EOC_{driving}$, EOC_{heat}, PP) (4E) perspectives was introduced in terms of different operating parameters.

- The proposed system can continuously provide 6 kW heating capacity with a PWHR over 0.8, and a COP_{sys} over 3.8 when considering the combined thermal management requirements for FC, battery, and cabin heating.

- The DRER of the designed system is at least 1.64 times the DRER of the reference EVASHP and 1.82 times the PTC baseline when providing the same amount of heat to the cabin. The maximum value of DR and DRER is highly dependent on the I_{FC} and B_{dch}, and it was determined that B_{dch} has a greater impact. The proposed system can always provide a stable heating load to the cabin with high COPsys by utilizing the waste heat from the battery pack and fuel cell stack. Meanwhile, the driving range is extended compared to vehicles that only have PTC or EVASHP thermal management systems. Great potential for improving the environment and lower operating costs can be achieved compared to vehicles with traditional thermal management systems. Details are concluded below:
- The exergy efficiency of the proposed system varies between 0.7 and 0.8 and it decreases with a decrease in ambient temperature but increases with an increase in fuel cell current output.
- Environmental analysis demonstrates that direct emission accounts for 88.7% and 43% of the total $TWEI_{hp}$ and $TEWI_{DR}$ respectively for the proposed system while direct emissions only account for 46% and 22% respectively for the reference EVASHP and PTC system.
- A lower GWP for the selected refrigerant will result in a greater improvement on the TWEI for the proposed system. Meanwhile, the ratio between β_{H2} and β_{elec} should meet a certain ratio in order to allow the proposed system to achieve a lower $TEWI_{DR}$ compared to the reference system, which in this case is, at most, 85%.
- The $EOC_{driving}$ and the EOC_{heat} of the proposed system is 4.9kWh/£ and 3.91 kWh/£ respectively at the simulation condition. This is 28.9% higher but 3.4% lower than the reference EVASHP system and 62% and 32.8% higher than the PTC baseline.
- The PP of the proposed system calculated based on the most up to date H_2 price when comparing to current EVs with ASHP and PTC is 300,000 km. However, it will reduce to 100,000 km when the price of H_2 is the same as electricity and the ACC of the proposed system is halved.

6. Outlook and future research

Going forward, further performance optimization should be conducted, and other components' heating or cooling demands considered. Different low GWP refrigerants should be applied and analysed in order to achieve lower environmental impacts. The optimal fuel cell size and fuel cell current output should be investigated to lower the capital cost and payback duration and increase the performance. Furthermore, a dynamic model could be built in Matlab Simulink and tested under widely adopted test cycles, such as Worldwide Harmonized Light Vehicles Test Cycle (WLTC). The main aim is to consider fuel cell and battery output and SOC together, in order to better understand the dynamic performance under different operating conditions. A test rig could be built to evaluate the practical performance and optimize our model. The cooling performance of the proposed system in the summer should be investigated and be compared to current published systems.

CRediT authorship contribution statement

Nan Zhang: Writing – original draft, Validation, Conceptualization, Methodology, Software. **Yiji Lu:** Conceptualization, Supervision, Writing – review & editing, Project administration, Funding acquisition. **Sambhaji Kadam:** Methodology, Validation, Writing – review & editing. **Zhibin Yu:** Conceptualization, Supervision, Funding acquisition, Resources.

Declaration of Competing Interest

The authors declare that they have no known competing financial interests or personal relationships that could have appeared to influence the work reported in this paper.

Data availability

Data will be made available on request.

Acknowledgements

The authors would like to acknowledge the support of EPSRC through their funding of the Decarbonisation of Heating and Cooling (EP/T022701/1) project and the ETP/Transport Scotland Industry Engagement Fund. This work was also funded by the University of Glasgow Studentship and China Scholarship Council (CSC) (202008230188). Finally, thanks to Ms. Lisa Smeaton for proofreading this manuscript (https://www.linkedin.com/in/lisa-smeaton-39357b19a/).

References

[1] Grant N. The Paris Agreement's ratcheting mechanism needs strengthening 4-fold to keep 1.5°C alive. Joule. 2022;6:703–8.
[2] Axsen J, Bhardwaj C, Crawford C. Comparing policy pathways to achieve 100% zero-emissions vehicle sales by 2035. Transp Res Part D: Transp Environ 2022;112:103488.
[3] Lauvergne R, Perez Y, Françon M, Tejeda De La Cruz A. Integration of electric vehicles into transmission grids: a case study on generation adequacy in Europe in 2040. Appl Energy 2022;326:120030.
[4] Zhang Z, Li W, Zhang C, Chen J. Climate control loads prediction of electric vehicles. Appl Therm Eng 2017;110:1183–8.
[5] Fetene GM, Kaplan S, Mabit SL, Jensen AF, Prato CG. Harnessing big data for estimating the energy consumption and driving range of electric vehicles. Transp Res Part D: Transp Environ 2017;54:1–11.
[6] Marcotte M, Grabowski S. 16 - Minimising energy consumption associated with drying, baking and evaporation. In: Klemeš J, Smith R, Kim J-K, editors. Handbook of water and energy Management in Food Processing. Woodhead Publishing; 2008. p. 481–522.
[7] Lee H-S, Lee M-Y. Steady state and start-up performance characteristics of air source heat pump for cabin heating in an electric passenger vehicle. Int J Refrigerat 2016;69:232–42.
[8] Lee D-Y, Cho C-W, Won J-P, Park YC, Lee M-Y. Performance characteristics of mobile heat pump for a large passenger electric vehicle. Appl Therm Eng 2013;50:660–9.
[9] Qin F, Xue Q, Albarracin Velez GM, Zhang G, Zou H, Tian C. Experimental investigation on heating performance of heat pump for electric vehicles at −20 °C ambient temperature. Energ Conver Manage 2015;102:39–49.
[10] Direk M, Yüksel F. Experimental evaluation of an automotive heat pump system with R1234yf as an alternative to R134a. Arab J Sci Eng 2019;45:719–28.
[11] Yu B, Ouyang H, Shi J, Guo Z, Chen J. Experimental evaluation of cycle performance for new-developed refrigerants in the electric vehicle heat pump systems. Int J Refrigerat 2021;129:118–27.
[12] Junqi D, Yibiao W, Shiwei J, Xianhui Z, Linjie H. Experimental study of R744 heat pump system for electric vehicle application. Appl Therm Eng 2021;183.
[13] Wang D, Yu B, Li W, Shi J, Chen J. Heating performance evaluation of a CO2 heat pump system for an electrical vehicle at cold ambient temperatures. Appl Therm Eng 2018;142:656–64.
[14] Yu B, Yang J, Wang D, Shi J, Guo Z, Chen J. Experimental energetic analysis of CO2/R41 blends in automobile air-conditioning and heat pump systems. Appl Energy 2019;239:1142–53.
[15] Qin F, Zhang G, Xue Q, Zou H, Tian C. Experimental investigation and theoretical analysis of heat pump systems with two different injection portholes compressors for electric vehicles. Appl Energy 2017;185:2085–93.
[16] Jung J, Jeon Y, Lee H, Kim Y. Numerical study of the effects of injection-port design on the heating performance of an R134a heat pump with vapor injection used in electric vehicles. Appl Therm Eng 2017;127:800–11.
[17] Yang T, Zou H, Tang M, Tian C, Yan Y. Experimental performance of a vapor-injection CO2 heat pump system for electric vehicles in −30 °C to 50 °C range. Appl Therm Eng 2022;217:119149.
[18] Steiner A, Rieberer R. Simulation based identification of the ideal defrost start time for a heat pump system for electric vehicles. Int J Refrigerat 2015;57:87–93.
[19] Zhou G, Li H, Liu E, Li B, Yan Y, Chen T, et al. Experimental study on combined defrosting performance of heat pump air conditioning system for pure electric vehicle in low temperature. Appl Therm Eng 2017;116:677–84.
[20] Li W, Liu Y, Liu R, Wang D, Shi J, Yu Z, et al. Performance evaluation of secondary loop low-temperature heat pump system for frost prevention in electric vehicles. Appl Therm Eng 2021;182.
[21] Liu N, Cui Q, Li H, Li K, Fang Y, Su L, et al. Investigating the performance optimization of an outdoor condenser–evaporator for an electric vehicle heat pump system. Energy Rep 2021;7:5130–40.
[22] Mahvi AJ, Boyina K, Musser A, Elbel S, Miljkovic N, Lab National Renewable Energy, et al. Superhydrophobic heat exchangers delay frost formation and enhance efficency of electric vehicle heat pumps. Int J Heat Mass Transf 2021;172:121162.

[23] Jung J, Jeon Y, Cho W, Kim Y. Effects of injection-port angle and internal heat exchanger length in vapor injection heat pumps for electric vehicles. Energy. 2020; 193:116751.
[24] Lu Y, Chen H, Wang L, Yu Z, Huang Y, Yu X, et al. Energy storage driving towards a clean energy future. Energy Rep 2021;7:8128–30.
[25] Ahn JH, Kang H, Lee HS, Jung HW, Baek C, Kim Y. Heating performance characteristics of a dual source heat pump using air and waste heat in electric vehicles. Appl Energy 2014;119:1–9.
[26] Han X, Zou H, Wu J, Tian C, Tang M, Huang G. Investigation on the heating performance of the heat pump with waste heat recovery for the electric bus. Renew Energy 2020;152:835–48.
[27] Tian Z, Gan W, Zhang X, Gu B, Yang L. Investigation on an integrated thermal management system with battery cooling and motor waste heat recovery for electric vehicle. Appl Therm Eng 2018;136:16–27.
[28] Tian Z, Gu B, Gao W, Zhang Y. Performance evaluation of an electric vehicle thermal management system with waste heat recovery. Appl Therm Eng 2020;169.
[29] Lee S, Chung Y, Jeong Y, Kim MS. Experimental study on an electric vehicle heat pump system with multi-level waste heat recovery using a vapor injection technique at low ambient temperatures. Energ Conver Manage 2022;267:115935.
[30] Albayati I, Ali R, Calay R. Modelling and examining open circuit voltage for PEM fuel cells. J Electrical Eng 2013;13:140–6.
[31] Wang Y, Wang C-Y. Modeling polymer electrolyte fuel cells with large density and velocity changes. J Electrochem Soc 2005;152:A445.
[32] Saleh IMM, Ali R, Zhang H. Simplified mathematical model of proton exchange membrane fuel cell based on horizon fuel cell stack. J Mod Power Syst Clean Energy 2016;4:668–79.
[33] Mann RF, Amphlett JC, Hooper MA, Jensen HM, Peppley BA, Roberge PR. Development and application of a generalised steady-state electrochemical model for a PEM fuel cell. J Power Sources 2000;86:173–80.
[34] Khan M, Iqbal M. Dynamic modeling and simulation of a small wind–fuel cell hybrid energy system. Renew Energy 2005;30:421–39.
[35] Liso V, Nielsen MP, Kær SK, Mortensen HH. Thermal modeling and temperature control of a PEM fuel cell system for forklift applications. Int J Hydrogen Energy 2014;39:8410–20.
[36] Larminie J, Dicks A. Fuel cell systems explained. 2nd ed. Chichester, West Sussex: J. Wiley; 2003.
[37] Hayes JG, Goodarzi GA. Electric powertrain: Energy systems, power electronics and drives for hybrid, electric and fuel cell vehicles. Hoboken, New Jersey: Wiley; 2018.
[38] Liu G, Ouyang M, Lu L, Li J, Han X. Analysis of the heat generation of lithium-ion battery during charging and discharging considering different influencing factors. J Therm Analys Calorim 2014;116:1001–10.
[39] Transportation USDO. New car assessment program (NCAP) FMVSS NO. 305 incidant test. 2013.
[40] Yan YY, Lin TF. Evaporation heat transfer and pressure drop of refrigerant R-134a in a plate heat exchanger. J Heat Transfer 1999;121:118–27.
[41] Donowski V. Theoretical investigation of the evaporation heat transfer coffifficient of refrigerant R-134a in a plate heat exchanger. Rochester Institute of Technology; 1999.
[42] Incropera FP, DeWitt DP. Fundamentals of heat and mass transfer. Wiley; 2002.
[43] Dobson MK, Chato JC. Condensation in smooth horizontal tubes. J Heat Transfer 1998;120:193–213.
[44] Wallis GB. Discussion: "estimation of steady-state steam void-fraction by means of the principle of minimum entropy production" (Zivi, S. M., 1964, ASME J. Heat Transfer, 86, pp. 247–251). J Heat Transfer 1964;86:252.
[45] Kinab E, Marchio D, Rivière P, Zoughaib A. Reversible heat pump model for seasonal performance optimization. Energ Buildings 2010;42:2269–80.
[46] Guo JJ, Wu JY, Wang RZ, Li S. Experimental research and operation optimization of an air-source heat pump water heater. Appl Energy 2011;88:4128–38.
[47] Cuevas C, Fonseca N, Lemort V. Automotive electric scroll compressor: testing and modeling. Int J Refrigerat 2012;35:841–9.
[48] Zaareer M, Mourad A-H. Effect of vehicle side Mirror Base position on aerodynamic forces and acoustics. Alex Eng J 2022;61:1437–48.
[49] Tesla. Models owner's manual. www.tesla.com.. Tesla; .
[50] Szirtes T. Applied dimensional analysis and modeling. Butterworth-Heinemann; 2007.
[51] Habermehl C, Jacobs G, Neumann S. A modeling method for gear transmission efficiency in transient operating conditions. Mech Machine Theory 2020;153: 103996.
[52] Xu J, Zhang C, Fan R, Bao H, Wang Y, Huang S, et al. Modelling and control of vehicle integrated thermal management system of PEM fuel cell vehicle. Energy. 2020;199.
[53] Rana T, Yamamoto Y. Universal electric vehicle thermal management system. SAE Int J Adv Curr Pract Mobil 2020;3:604–13.
[54] Dai B, Liu C, Liu S, Wang D, Wang Q, Zou T, et al. Life cycle techno-enviro-economic assessment of dual-temperature evaporation transcritical CO2 high-temperature heat pump systems for industrial waste heat recovery. Appl Therm Eng 2023;219:119570.
[55] Leo TJ, Durango JA, Navarro E. Exergy analysis of PEM fuel cells for marine applications. Energy. 2010;35:1164–71.
[56] Amidpour M, Khoshgoftar Manesh MH. Chapter 5 - exergy and thermoeconomic evaluation of cogeneration and polygeneration systems. In: Amidpour M, Khoshgoftar Manesh MH, editors. Cogeneration and Polygeneration systems. Academic Press; 2021. p. 55–74.
[57] Kadam ST, Kyriakides A-S, Khan MS, Shehabi M, Papadopoulos AI, Hassan I, et al. Thermo-economic and environmental assessment of hybrid vapor compression-absorption refrigeration systems for district cooling. Energy. 2022;243:122991.
[58] Koronaki IP, Cowan D, Maidment G, Beerman K, Schreurs M, Kaar K, et al. Refrigerant emissions and leakage prevention across Europe – results from the RealSkillsEurope project. Energy. 2012;45:71–80.
[59] Wu J, Zhou G, Wang M. A comprehensive assessment of refrigerants for cabin heating and cooling on electric vehicles. Appl Therm Eng 2020;174:115258.
[60] O'Neill NF, Ma JM, Walther DC, Brockway LR, Ding C, Lin J. A modified total equivalent warming impact analysis: addressing direct and indirect emissions due to corrosion. Sci Total Environ 2020;741:140312.
[61] Ember.. Carbon intensity of the power sector in the European Union in 2021, by country (in grams of CO_2 per kilowatt-hour). www.statista.com.. Statista; .
[62] Rievaj V, Gaňa J, Synák F. Is hydrogen the fuel of the future? Transp Res Procedia 2019;40:469–74.
[63] Washers KP. Mini 12v (DC) Submersible Water Pump To Run 10/122 From Tank. https://kranzle-pressure-washers.co.uk/products/mini-12v-submersible-water-pump2022; 2023.
[64] Beijing Golden Nanfeng International Manufacturer TC. High Voltage Electric Vehicle PTC heater similar to Webasto high-voltage heater (HVH) for electric and hybrid vehicles. https://www.alibaba.com/product-detail/High-Voltage-Electric-Vehicle-PTC-heater_1600504411156.html2022.
[65] Institute BM. Manufacturing cost analysis of PEM fuel cell systems for 5- and 10-kW backup power applications. U.S. Department of Energy; 2016.
[66] Hua T, Ahluwalia R, Peng J-K, Kromer M, Lasher S, McKenney K, et al. Technical assessment of compressed hydrogen storage tank Systems for Automotive Applications United States. Argonne National Laboratory; 2010.
[67] Duffner F, Wentker M, Greenwood M, Leker J. Battery cost modeling: a review and directions for future research. Renew Sustain Energy Rev 2020;127:109872.
[68] Ajanovic A, Glatt A, Haas R. Prospects and impediments for hydrogen fuel cell buses. Energy. 2021;235:121340.
[69] Energy bills support factsheet. In: GOV.UK, editor. Department for Business EIS, editor. GOV.UK: GOV.UK; 2022.
[70] Lee H, Lee D, Kim Y. Heating performance of a coolant-source heat pump using waste heat from stack and electric devices in fuel cell electric vehicles under cold conditions. Energ Conver Manage 2022;252:115092.
[71] Candelaresi D, Valente A, Bargiacchi E, Spazzafumo G. 16 - life cycle assessment of hybrid passenger electric vehicle. In: Lo Faro M, Barbera O, Giacoppo G, editors. Hybrid Technologies for Power Generation. Academic Press; 2022. p. 475–95.
[72] Hao X, Wang H, Lin Z, Ouyang M. Seasonal effects on electric vehicle energy consumption and driving range: a case study on personal, taxi, and ridesharing vehicles. J Clean Prod 2020;249:119403.